EEET ECOLOGICAL ENGINEERING & ENVIRONMENTAL TECHNOLOGY

Ecological Engineering & Environmental Technology, 2026, 27(3), 341–367
https://doi.org/10.12912/27197050/218187
ISSN 2719–7050, License CC-BY 4.0

Received: 2026.01.28
Accepted: 2026.02.25
Published: 2026.03.01

Land cover change and urban growth in north Gorontalo Regency using Sentinel-2 imagery

Nur Wandani Risanty Elisa Marta Irwan Djafar[1], Andang Suryana Soma[2*], Mahmud Achmad[3], Lalu Kharismananda Hakiki[1]

[1] Regional Planning and Development Study Program, Postgraduate School, Hasanuddin University, Makassar, Indonesia
[2] Department of Forestry, Faculty of Forestry, Hasanuddin University, Makassar, Indonesia
[3] Department of Agricultural Technology, Faculty of Agricultural Technology, Hasanuddin University, Makassar, Indonesia
* Corresponding author e-mail: s_andangs@unhas.ac.id

ABSTRACT

Land cover change reflects regional development dynamics driven by urbanization and infrastructure expansion and may lead to inconsistencies with the Regional Spatial Plan (RTRW). The objective of this study is to identify spatiotemporal patterns of land cover change and urban growth in north Gorontalo Regency using Sentinel-2 imagery and vegetation indices (NDVI and NDLI), and to evaluate their consistency with the regional spatial plan (RTRW). The analysis employed Sentinel-2A imagery from 2016 and 2025 via a spatial–temporal approach. The land cover classification accuracy was assessed via a confusion matrix, whereas the urban growth direction was analyzed via the standard deviational ellipse (SDE). Land cover change modeling was conducted via the CLUE-S model with a weight-of-evidence (WoE) approach, and the results were validated via receiver operating characteristic (ROC) curves. The results indicate that built-up areas increased by approximately 1,470 ha (82.12%) between 2016 and 2025, mainly through the conversion of agricultural land and fishponds. Urban expansion exhibits a dominant east–southeast orientation, forming a linear pattern along major transportation corridors. The integrated use of NDVI and NDLI identifies vegetation–nonvegetation transition zones, capturing early-stage urban encroachment that is not detected using NDVI alone. Modeling results show that NDVI and distance to roads are the primary drivers of land cover change, while elevation and distance to government centers are secondary. The CLUE-S model performs well, with an overall accuracy of 98.79%, a kappa coefficient of 0.78, and an ROC value of 0.71. This study is limited by the use of two temporal observations and the exclusion of dynamic socioeconomic variables. Scientifically, the findings demonstrate that integrating NDVI–NDLI analysis with CLUE-S–WoE modeling reveals spatiotemporal urban growth patterns and driving mechanisms beyond conventional single-index approaches, while providing a quantitative basis for improving RTRW evaluation.

Keywords: land cover change; NDVI; NDLI; CLUE-S; urban growth direction; north Gorontalo Regency.

INTRODUCTION

Land cover change results from complex interactions between human activities and land resources (Rakuasa & Pakniany, 2022; Latue et al., 2023) and has become a critical issue in regional planning, particularly in developing areas experiencing population growth and urbanization. This process is commonly reflected in the conversion of vegetated and agricultural land into built-up areas, which may reduce environmental carrying capacity and lead to mismatches between spatial planning policies and actual land use conditions.

North Gorontalo Regency is one of the regions exhibiting increasingly dynamic development. According to data from Badan Pusat Statistik Gorontalo Utara (BPS, 2025), the population growth rate was recorded at 1.47% in 2022, increased to 1.51% in 2023, and rose again

to 1.53% in 2024. This trend indicates growing pressure on land demand, housing, infrastructure, and urban space. However, compared with other regions in Gorontalo province, population density in north Gorontalo remains relatively low(BPS, 2025), suggesting that the region is still in an early phase of urban development and represents a strategic area for spatial guidance, particularly as the regency spatial plan (RTRW) is currently undergoing revision.

Remote sensing based on Sentinel-2 imagery enables spatial-temporal monitoring of land cover change (Nagendra et al., 2004; Juniyanti et al., 2020) through vegetation indices such as NDVI and NDLI (Putri et al., 2021). Kawamuna et al. (2017) and Rakhmat Awaliyan et al. (2018) described Sentinel-2 as a satellite system comprising 13 spectral bands, including four bands with 10-m resolution, six bands with 20-m resolution, and three bands with 60-m spatial resolution, with a swath width of 290 km. These characteristics allow more precise identification of vegetation degradation, settlement expansion, and vegetation–non-vegetation transition zones compared to other satellite imagery.

Numerous previous studies have developed land use change and urban growth modeling at metropolitan, regional, and biome scales, such as the work of (da Rocha de Souza et al., 2025) in Brazil and Portugal, (Varnier & Weber, 2025) across three Brazilian biomes, and (Giofandi et al., 2025), who integrated CLUE-S with driving factors at the watershed scale. Scenario-based modeling approaches have also been widely applied using Dinamica EGO (Pinto et al., 2025); (Gonzales & Hopfgartner, 2024). In Indonesia, however, most studies remain descriptive or focus on specific objects, such as land cover change in Ambon City (Latue et al., 2023), NDVI analysis in educational forests (Setiawan & Rijal, 2024), Sentinel-2 land cover classification using NDVI and random forest (Marlina, 2022), and NDVI-based mangrove vegetation density change (Dharma et al., 2022).

Specifically in north Gorontalo, studies on land cover change are still very limited and fragmented. Research by (Wahdaniah, Sukirman Rahim, 2022) focused only on the impacts of industrial plantation forests in Monano District, while (Baderan, 2017) examined mangrove ecosystem degradation in Kwandang District. To date, no study has comprehensively investigated land cover change and urban development direction at the administrative scale of north Gorontalo Regency by integrating vegetation biophysical dynamics with spatial modeling.

Addressing this research gap, the present study proposes an integrated NDVI–NDLI approach combined with CLUE-S modeling to detect early vegetation–non-vegetation transition zones while simultaneously identifying urban growth directions in north Gorontalo Regency. The main novelty of this research lies in coupling vegetation biophysical dynamics with spatial modeling and directly evaluating the regional spatial plan (RTRW), thereby revealing the structural mechanisms of settlement expansion in semi-rural areas. This study also assumes that infrastructure accessibility plays a dominant role in shaping urban growth patterns, and its results are expected to provide a spatially based scientific foundation for more adaptive and sustainable regional planning.

RESEARCH METHODS

Research location

This study was conducted within the administrative area of north Gorontalo Regency, Gorontalo Province, which is divided into 11 districts. north Gorontalo Regency extends longitudinally in an east-west direction across the northern part of Gorontalo province, following the northern section of the Trans-Sulawesi road corridor. Geographically, the mainland area of north Gorontalo Regency is located between 386,732–530,446 mE and 74,367–115,085 mN (UTM Zone 51 North). The research location map is shown in Figure 1.

Materials and methods

Geospatial Dataset

The study employs Sentinel-2A imagery (January 2016–November 2025; 10–20% cloud cover) acquired from Copernicus, together with supporting spatial layers for Kabupaten Gorontalo Utara. Image preprocessing and variable extraction were performed in ArcGIS developed by Esri to derive NDVI, NDLI, and accessibility-related drivers. The statistical significance of driving factors was assessed using binary logistic regression implemented in software developed by IBM (SPSS) in the

study (Pandapotan Sinurat et al., 2015) Spatial patterns of built-up expansion were examined using the Standard Deviational Ellipse as conducted by (Cao & Kim, 2025), while land cover change was simulated using the CLUE-S model implemented through Dinamica EGO in the study Akın et al. (2022) and Jiang et al. (2015). Model outputs were subsequently overlaid with the regional spatial plan (RTRW) as a policy constraint to evaluate the spatial consistency of urban growth trajectories. Dataset specifications and the analytical workflow are summarized in Table 1 and Figure 2.

Land cover change analysis

Image classification

Land cover conditions for 2016 and 2025 in Kabupaten Gorontalo Utara were derived from Sentinel-2A imagery processed in ArcGIS developed by Esri using supervised classification (Maximum Likelihood Classification) following (Ardianto et al., 2022) approach and change detection techniques, referring to the framework of (Badan Standardisasi Nasional, 2010). Training samples were manually selected based on visual image interpretation and supported by field verification to ensure consistency with actual land cover and vegetation conditions.

Accuracy test

The validation points are manually selected by researchers and distributed to each sub district according to the designated land cover class. In her research Novianti (2021), she discussed land cover classification accuracy testing via an error matrix. The matrix is square shaped, with the numbers in the rows and columns corresponding to the classification accuracy category being assessed. Image classification is considered correct if the confusion matrix calculation is >75%. The confusion matrix calculation can be seen in Table 4.

The accuracy parameters calculated from the confusion matrix are as follows:
a) Overall accuracy (OA),

Table 1. Data requirements

Data required	Data sources	Outputs
Sentinel-2A imagery (April 2016 and November 2025 datasets)	Dataspace.copernicus.eu	Multispectral base imagery with 10 m spatial resolution
Administrative boundary of North Gorontalo Regency	RTRW North Gorontalo Regency 2011-2031 (PUPR)	Administrative boundary layer for image clipping
Sampling points	Visual interpretation of high-resolution Google Earth imagery	Training samples and accuracy assessment
Visual validation data (Google Earth)	Visual interpretation of high-resolution Google Earth imagery	Visual validation of locations showing significant land cover changes
NDVI (Normalized Difference Vegetation Index)	from Sentinel-2A (2016 & 2025)	Red (B4) and Near-Infrared (B8) bands for NDVI calculation
NDLI (Normalized Difference Latent Index)	from Sentinel-2A (2016 & 2025)	Shortwave Infrared (B11) and NIR (B8A) bands for NDLI calculation
NDVI difference map (ΔNDVI)	Overlay result of NDVI 2025 minus NDVI 2016	Vegetation change map showing degradation/ development
NDLI difference map (ΔNDLI)	Overlay result of NDLI 2025 minus NDLI 2016	Map of land moisture changes (waterproof cover indicator)
Cardinal direction grid	Manually created in Arcgis (like an 8-way or 16-way compass)	Dividing the study area into cardinal direction zones from a central point to analyze the dominant direction of land cover change.
Land Cover Map (classification results)	Processed from Sentinel-2 imagery using NDVI and NDLI	Land cover change layers (2016–2025)
Elevation Map	North Gorontalo RTRW 2011-2031 (PUPR)	Elevation maps as biophysical driving variables
Distance to Main Road	North Gorontalo RTRW 2011-2031 (PUPR)	Biophysical and socioeconomic driving factor variables
Distance to Government Center	North Gorontalo RTRW 2011-2031 (PUPR)	Socioeconomic accessibility variables (social driving factors)
Official Land Use Map (RTRW)	North Gorontalo RTRW 2011-2031 (PUPR)	Comparison layer or zone restriction in modeling
Validation (most recent data of the simulation year)	Classification results data vs. most recent reference data (google earth pro)	Model accuracy, validation of prediction results

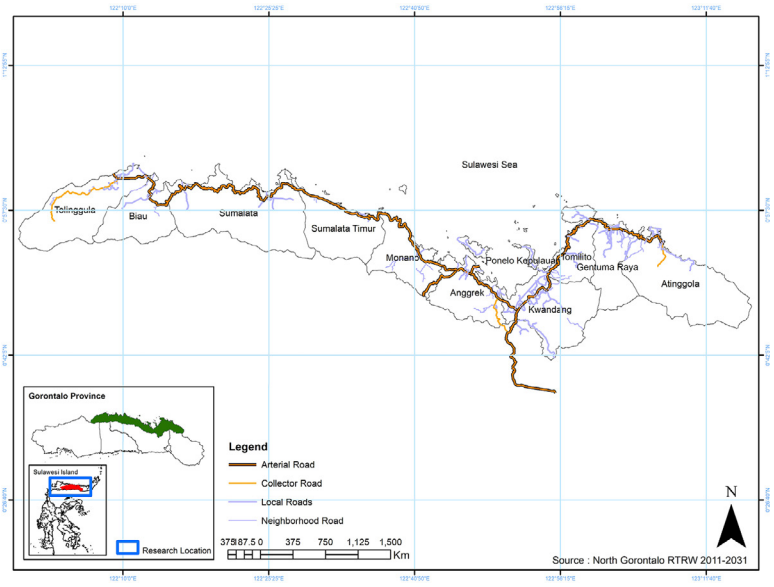

Figure 1. Map of the study location

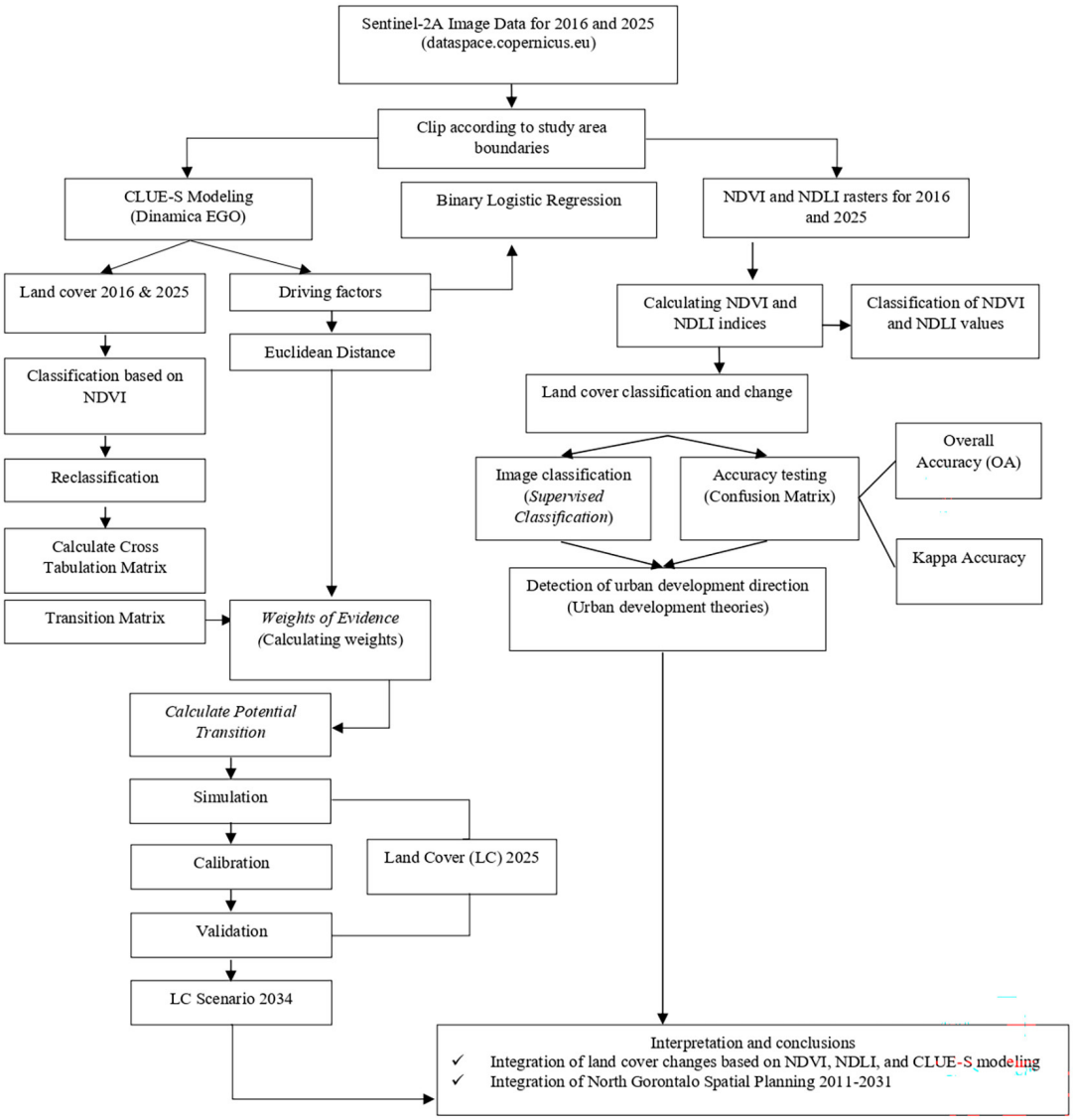

Figure 2. Analysis stage flowchart

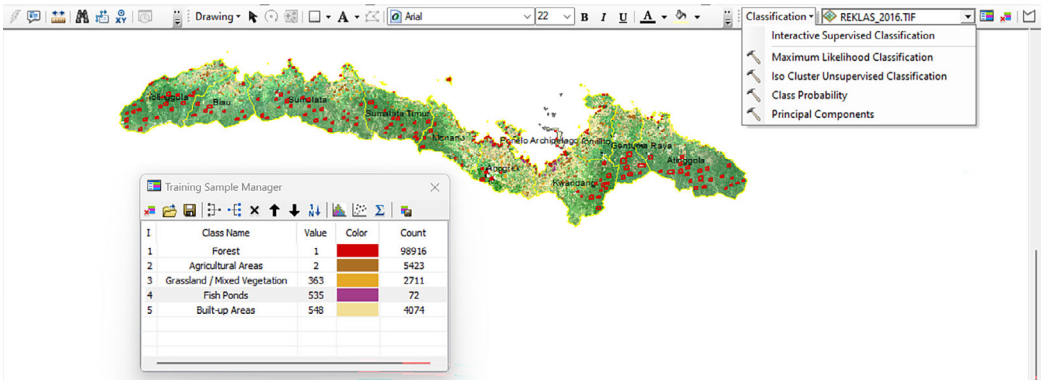

Figure 3. Training sample

Table 2. Land cover classes

Land cover classes	Descriptions
Vegetated	
Forest	Includes dryland forests (from lowland to mountainous areas), wetland forests (swamps, brackish swamps, and peat swamps influenced by tides or seasonal changes), and coastal mangrove forests, often modified by human activities.
Agricultural areas	Lands cultivated for food crops and horticulture, where natural vegetation has been replaced by anthropogenic crops requiring continuous human management, including plantations, rice fields, and dryland farms; these areas may be temporarily bare between growing seasons.
Grassland/mixed vegetation	Open dryland areas dominated by low natural vegetation (grasses and shrubs), with heterogeneous to homogeneous cover ranging from sparse to dense, typically representing former forest areas.
Un-Vegetated	
Built-up areas	Artificial and generally impervious surfaces replacing natural or semi-natural cover, including settlements, road networks, railways, airports, and seaports.
Fish ponds	Coastal aquaculture areas characterized by embankment patterns surrounding pond units.

Note: Badan Standardisasi Nasional, 2010,

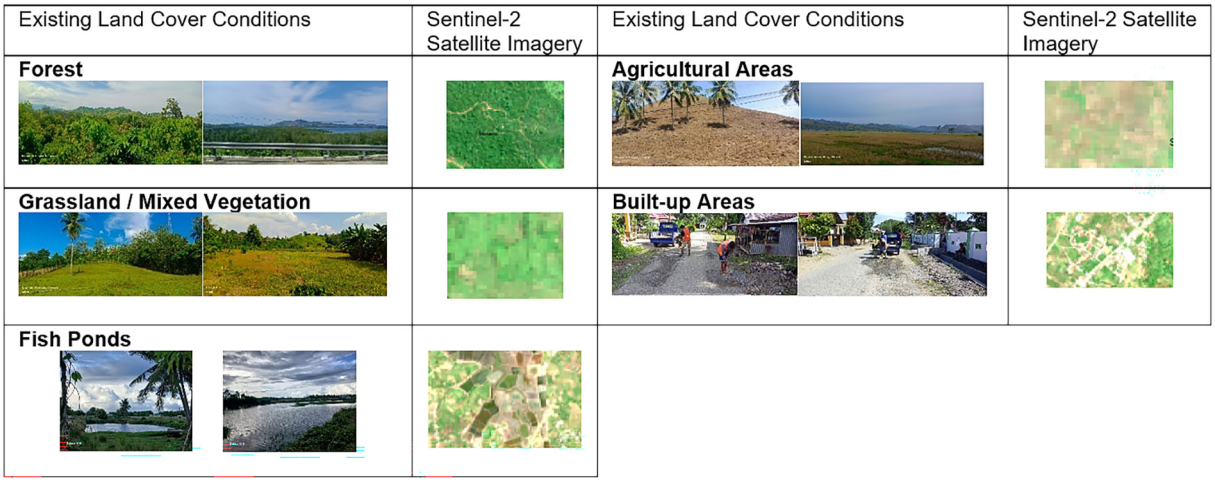

Figure 4. Training sample (Author's documentation, 2025)

The percentage of correct classifications of the total sample points is indicated.

$$(\sum_{i=1} \text{Xii})/\text{N}) \text{ X } 100\% \quad (1)$$

b) Kappa coefficient,

The classification accuracy is indicated by considering the agreement beyond random chance.

$$[(N \sum_{i=1}^{r} Xii - \sum_{i=1}^{r} X1 + X + 1) / /(N2 - \sum_{i=1}^{r} X1 + X + 1)] \times 100\% \quad (2)$$

where: *N is the* number of pixels in the sample, *X1+ is the* number of pixels in row-I, *X+1* is the number of pixels in column-I, *and Xii* is the diagonal value of the contingency matrix of row-i and column-i.

Furthermore, the kappa value is classified to assess the reliability of land cover classification by accounting for agreements that may occur by chance. Kappa values were used to assess model accuracy, where values < 0.4 indicate poor accuracy, 0.4–< 0.75 indicate medium accuracy, and > 0.75 indicate excellent accuracy Rahmawati et al. (2025).

Analysis of index changes

Normalized difference vegetation index

Syifa Putri et al. (2021) explained the theory of Sentinel-2 image interpretation by calculating the NDVI obtained by calculating near-infrared waves with red waves reflected by plants (Wahrudin et al., 2019). The NDVI method is capable of identifying plant cover through processed image computation (Purboyo et al., 2021). For the Sentinel-2 images, the images used for NDVI processing are Band 4 with red waves and Band 8 with near-infrared (NIR) waves. Producing vegetation maps and identifying areas with changes in vegetation cover in 2016 and 2025. The NDVI calculations use the following formula.

$$NDVI = \frac{(\mathrm{NIR} - \mathrm{Red})}{(\mathrm{NIR} + \mathrm{Red})} \quad (3)$$

where: NIR is the near-infrared reflectance (usually Band 8 on Sentinel-2), red is the red spectrum reflectance (Band 4 on Sentinel-2), and the NDVI values range from -1 (no vegetation) to +1 (dense vegetation).

After the NDVI and NDLI values are obtained, the next step is to interpret the NDVI and NDLI values in 2016 and 2025 on the basis of the classification in Table 5.

Normalized difference latent index

The NDLI has been proven to be an effective indicator for assessing the potential for surface evapotranspiration. Surface evapotranspiration reflects water availability and land moisture conditions. The advantage of the NDLI lies in its unique ability to optimize spectral sensitivity to land surface biophysical parameters by combining three spectral channels commonly used in satellite missions, namely, green, red, and shortwave infrared (SWIR) channels. The NDLI value is calculated via the following equation.

$$NDLI = \frac{(\mathrm{NIR} - \mathrm{SWIR})}{(\mathrm{NIR} + \mathrm{SWIR})} \quad (4)$$

Band 8 is used as the NIR value. Band 11 is used as the SWIR value. NDLI values range from -1 to +1. A value closer to 1 indicates high water availability (very moist), and a value closer to -1 (very dry) indicates low water availability (Nursaputra et al., 2021). Next, the NDLI values

Table 3. Confusion matrix

Reference class	Classified to class (classification data on map)			Number of pixels	Maker accuracy
	A	B	C		
A	X_{11}	X_{12}	X_{13}	X_{1+}	$X_{11/X1+}$
B	X_{21}	X_{22}	X_{23}	X_{2+}	$X_{22/X2+}$
C	X_{31}	X_{32}	X_{33}	X_{3+}	$X_{33/X3+}$
Total pixels	X_{+1}	X_{+2}	X_{+3}	N	
User accuracy	X_{11}/X_{+1}	X_{22}/X_{+2}	X_{33}/X_{+3}		

Note: Arisondang et al., 2015; Novianti, 2021.

Table 4. Classification of the NDVI and NDLI values

NDVI values	Interpretation	NDLI value	Interpretation
-1 s/d -0.03	Nonvegetated land	> 0.4	Very moist
-0.04 s/d 0.15	Very low vegetation	0.2–0.4	Moist
0.16 s/d 0.25	Low greenery	0–0.2	Moderately moist
0.26 s/d 0.35	Moderate greenery	-0.2–0	Dry
0.36 s/d 1.00	High greenery	< -0.2	Very dry

Note: NDVI – P.12/Menhut-II, 2012; Putri et al. (2021), NDLI – Meena et al. (2019).

for 2016 and 2025 are classified to visualize them in a raster map with a color scale.

Differences in the NDLI can be identified by calculating the change in the NDLI value (the difference between 2025 and 2016). A decrease in the NDLI indicates increased moisture or vegetation growth. An increase in the NDLI indicates drying, deforestation, or development.

Accuracy test

During accuracy assessment, the classification was simplified into general classes – vegetated and nonvegetated areas for the NDVI and moist and dry areas for the NDLI – to reduce spectral overlap and ensure consistency with reference data (Azizah Nazhifah et al., 2025). Accuracy testing was conducted via 100 validation points in each subdistrict, resulting in a total of 1,100 sampling points across 11 subdistricts. The NDVI and NDLI classification results were evaluated via a confusion matrix to calculate the overall accuracy (OA) and the kappa coefficient, which measure the overall classification performance and the level of agreement with reference data while accounting for random agreement.

Analysis of city direction and development

The analysis of urban development direction was conducted through an integrated spatial approach combining vegetation indices (NDVI and NDLI), built-up land change during 2016–2025, accessibility variables, and topographic factors. The workflow was designed to ensure reproducibility and was implemented sequentially in ArcGIS version 10.8.2.

Preparation of input spatial datasets

Sentinel-2 imagery from 2016 and 2025 was used to produce land cover maps and calculate NDVI and NDLI, with built-up expansion defined as pixels changing from non-built-up to built-up. Additional driving factors-distance to roads, distance to government centers, and

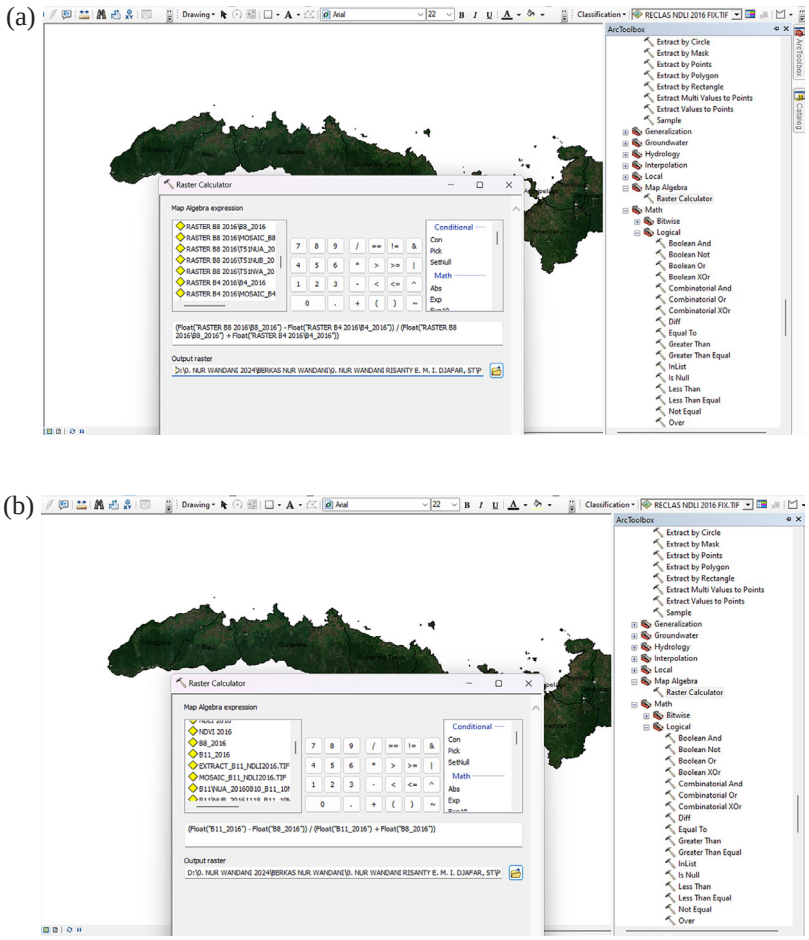

Figure 5. NDVI and NDLI calculation using raster calculator in ArcGIS based on Sentinel-2 imagery (a) extraction NDVI, (b) extraction NDLI

(a)

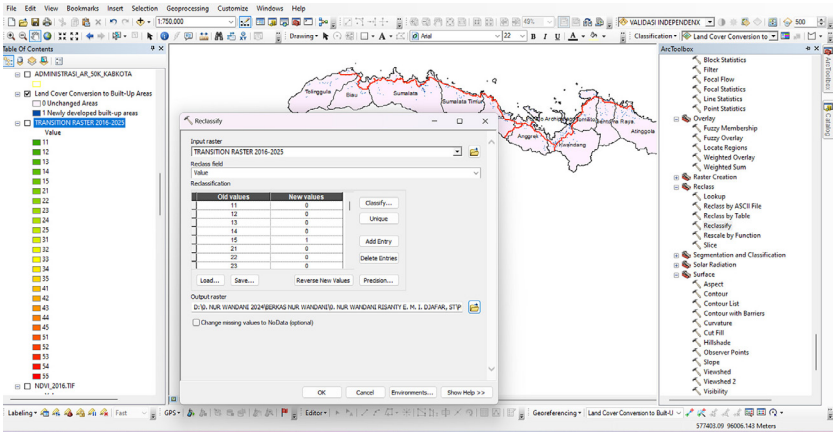

(b)

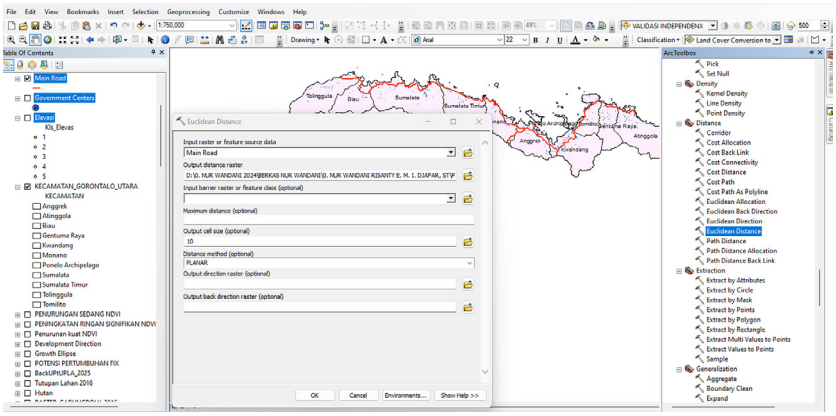

(c)

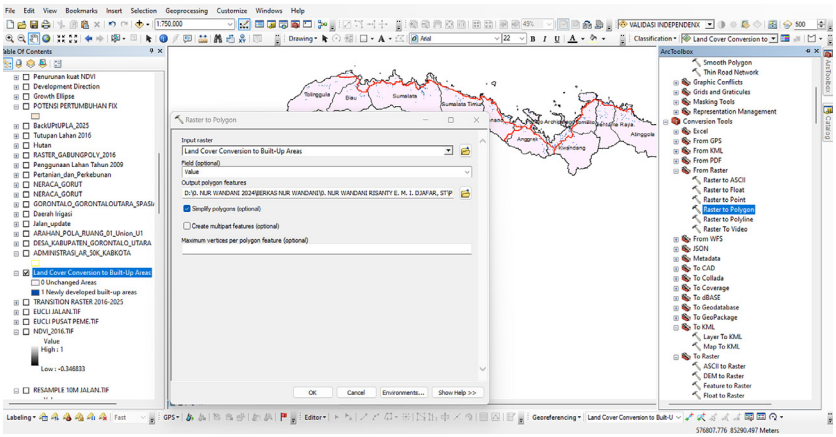

(d)

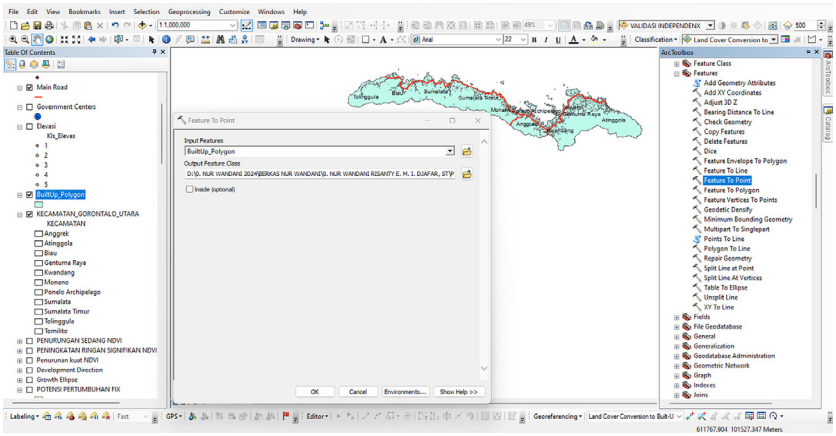

(e)

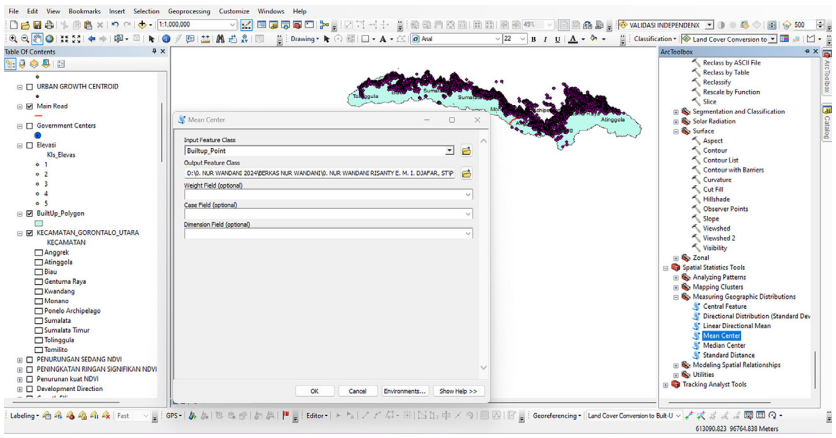

(f)

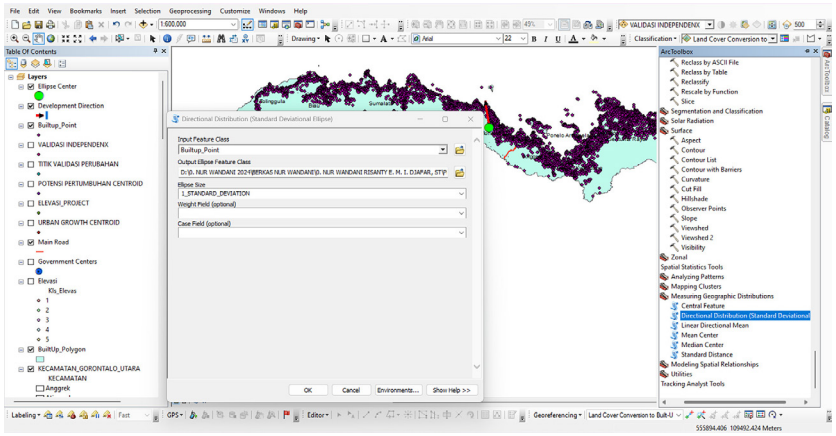

Figure 6. SDE of built-up expansion showing dominant growth orientation, (a) binary transition raster showing built-up (1) and no-change (0), (b) Euclidean distance, (c) raster to polygon, (d) feature to point, (e) mean center, (f) directional distribution (standard deviational)

elevation–were included to represent accessibility, administrative influence, and physical constraints. All raster datasets were standardized to UTM Zone 51N, 10 m resolution, and consistent extent for spatial analysis.

Raster overlay and identification of built-up expansion

Standardized rasters (NDVI, NDLI, built-up change, distance to roads, distance to government centers, and elevation) were overlaid to support spatial interpretation of urban expansion patterns. Pixels representing newly developed built-up areas between 2016 and 2025 were converted into point features using the Raster to Point tool. These growth points served as the primary dataset for subsequent directional analysis.

Determination of urban growth centroid

The spatial mean center (urban growth centroid) was calculated from built-up change points using the Mean Center tool. This centroid represents the average geographic location of urban expansion and was used as a reference point for assessing development direction.

Directional distribution analysis

Urban growth direction was quantified using the directional distribution (standard deviational ellipse, SDE) method with one standard deviation to characterize the spatial dispersion and directional trend of growth points. When the spatial pattern of features approximates a spatial normal distribution, with the highest density near the center and decreasing toward the edges, a one–standard deviation ellipse encompasses approximately 68% of the input features (feature centroids) (Esri, 2025). The SDE generates an ellipse defined by the mean center of distribution, major axis (maximum spatial variance), minor axis (minimum spatial variance), and rotation angle (azimuth). The rotation angle, measured

clockwise from geographic north (0–360°), indicates the dominant orientation of urban expansion, where values approaching 0° or 180° represent north–south trends and values near 90° or 270° indicate east–west development. Ellipse parameters including CenterX, CenterY, XStdDist, YStdDist, Rotation, Shape_Length, and Shape_Area were extracted to quantify spatial dispersion and directional tendencies following (Cao & Kim, 2025). To validate the SDE-derived growth direction, angular orientation was cross-checked through visual inspection of built-up density gradients and spatial clustering patterns.

Visualization and interpretation of urban growth patterns

Results from centroid and SDE analyses were visualized as urban development direction maps showing growth centers, spatial dispersion, and dominant expansion orientation. These outputs were interpreted in relation to road networks, government centers, and topographic conditions.

Observed spatial patterns were further evaluated using established urban growth theories, including the Concentric Zone Model (Burgess, 1925), Sector Model (Hoyt, 1939), and Multiple Nuclei Model (Harris & Ullman, 1945), as well as urban sprawl concepts (Ewing, 1997), to explain the underlying development mechanisms.

Land cover change modeling with CLUE-S

Binary logistic regression

The emergence of a particular type of land use is thought to be influenced by biogeophysical and socioeconomic factors (Warlina, 2011). The probability of land use change is analyzed via binary logistic regression with the forward stepwise method, which aims to eliminate insignificant influencing factors in the model. Binary logistic regression is a regression model where the dependent variable is binary or dichotomous to determine whether there is an influence of the independent variable (X) on the dependent variable (Y). The regression function is a monotonic response curve line bounded between 0 and 1 with the logistic function in the following equation (Pandapotan Sinurat et al., 2015).

$$Pi = E(Y) = (Exp(\beta_0 + \beta_1 X_1 + \beta_2 X_2 + ... + \beta_n X_i))/ /(1 + Exp(\beta_0 + \beta_1 X_1 + \beta_2 X_2 + ... + \beta_n X_i)) \quad (5)$$

where: Pi is the probability value of increasing land use cells, $E(Y)$ is the value obtained from the binary dependent variable Y, β_0 is the estimated constant value, and β_n is the estimated coefficient of each independent variable X_i (Gil Pontius Jr & Schneider, 2001; Pandapotan Sinurat et al., 2015).

The dependent variable consisting of each land use class is transformed into a binary raster map (0 and 1) with a pixel resolution of 100 × 100 meters. A value of 1 indicates one land use class, whereas a value of 0 indicates no land use. The independent variables in the form of biophysical and socioeconomic factors are classified on the basis of the category class of each data type from the smallest to the largest value via the natural breaks classification method in raster format with the same pixel resolution as the land use class (Pandapotan Sinurat et al., 2015).

The accuracy of the logistic regression model was evaluated using the ROC method, with values ranging from 0.5 to 1, where higher values indicate better model performance and spatial prediction accuracy. ROC values of 0.5–0.7 indicate low accuracy, 0.7–0.9 indicate good and reliable accuracy, and values above 0.9 reflect high precision (Manel et al., 2001; Jiang et al., 2015).

Data preparation

Land use change in Dinamica EGO was modeled using 2016 and 2025 Sentinel-2A land cover maps (10 m resolution) derived via NDVI and NDLI indices in ArcGIS, covering a nine-year historical period and projected for 2025–2034. All datasets were reclassified into model-specific categories, standardized in resolution and UTM Zone 51 N, and stored as raster (.tif). Driving factors – elevation, distance to roads, and distance to government centers – were analyzed with Euclidean distance and evaluated via the weights of evidence (WoE) method to assess their spatial influence on land cover change.

Calculation of the cross-tabulation matrix

In Dinamica EGO land cover change modeling, a cross-tabulation matrix quantifies class transitions between the 2016 (initial) and 2025 (final) maps. Cell-by-cell comparison records each class change as a frequency in a two-dimensional matrix. This matrix forms the basis for estimating the probability and magnitude of land cover change in subsequent simulations.

Transition matrix

After cross-tabulation, Dinamica EGO modeling proceeds with preparing a transition matrix that quantifies changes between land cover classes over a given period. Rows represent initial classes and columns represent target classes. The matrix is expressed in absolute cell counts or proportions according to modeling needs.

Weights of evidence

This method determines land cover transition probabilities on the basis of Bayesian probability by linking the presence of driving factors to the likelihood of land use change (Eastman et al., 2005;Gonzales & Hopfgartner, 2024). Each land-use/land-cover transition is analyzed individually by classifying driving factors, such as distance to roads, elevation, slope, distance to urban centers, and socioeconomic variables, into specific intervals or classes. Logarithmic weights are then calculated from the frequency distribution of transition locations within each class, producing positive weights (W+), which indicate conditions that increase the probability of change, and negative weights (W−), which represent conditions that inhibit land cover transitions (Riaz et al., 2024).

Calculation of the transition potential

In general, the transition potential is a probabilistic value assigned to each pixel or cell within a study area, indicating how likely it is that the cell will experience a change from one land cover class to another, as defined in the transition matrix. This value is calculated by accumulating the weights (both W+ and W−) generated in the Weights of Evidence stage for each driving factor relevant to the transition.

Simulation

The next step in modeling with Dinamica EGO is to run a land cover change simulation. This stage is the core of spatial modeling, where the system replicates the dynamics of land cover change for the time period from 2016–2025. In the simulation process, Dinamica EGO uses information from several main components and a transition matrix, which determines the number of cells that will change from one class to another. Transition potential map, which shows the most likely location for change to occur.

Calibration

Calibration was conducted to refine model parameters so that simulated land use changes matched historical patterns. Using only the 2016 and 2025 maps, this involved adjusting the transition matrix, optimizing weights of evidence (WoE), and tuning cellular automata parameters such as patch size, expansion, and compactness. Iterative testing continued until the simulated results closely reflected the observed spatial patterns and magnitude of land use change.

Validation

After calibration, the model is validated by comparing the simulated 2025 map with the actual 2025 map. Accuracy is assessed using metrics such as overall accuracy, which measures the percentage of correctly classified pixels, and the kappa statistic, which accounts for agreement beyond chance. Validation can be performed in Dinamica EGO using the Compare Maps module or with software like ArcGIS for more detailed spatial analysis.

Scenario

After adjusting all scenario parameters, Dinamica EGO and ArcGIS run the spatial simulation to produce a predicted 2034 land cover map. Simulations can be repeated to compare different scenarios, such as business-as-usual (BAU), assuming trends continue without intervention, and ecological protection, reflecting the effects of conservation policies.

RESULTS AND DISCUSSION

Land cover conditions

Land cover conditions in 2016 and 2025

Land cover change analysis from 2016–2025 revealed significant shifts among land cover classes. The forest area slightly increased by 2.17 ha (2.16%), whereas the agricultural land area decreased by 8.72 ha (24.85%). Grassland or mixed vegetation expanded by 9.21 ha (33.26%), whereas pond aquaculture declined substantially by 131 ha (45.64%). Built-up land showed the most pronounced change, increasing by 1,470 ha (82.12%), indicating rapid urban and infrastructure development during the study period. The land cover conditions in 2016 and 2025 are shown

in Table 6. Furthermore, the land cover conditions in 2016 and 2025 are shown in Figure 7.

To ensure the quality of the land cover classification results, an accuracy test was conducted via a confusion matrix. A total of 3,901 sample points were manually distributed in each subdistrict for each land cover class, which served as reference data to assess the suitability of the classification results to actual conditions in the field. The land cover confusion matrix for 2016 is shown in Table 7.

The reliability of the 2025 land cover classification results was ensured by conducting an accuracy test using field reference data and Google Earth imagery from 2025 via a confusion matrix approach. The validation process used 3,435 manually distributed sample points across each subdistrict for each land cover class, as shown in Table 8.

The accuracy assessment revealed that both the 2016 and 2025 land cover classifications were of high quality. The 2016 classification achieved an overall accuracy (OA) of 93%, with a kappa coefficient of 0.91, whereas the 2025 classification achieved an OA of 92%, with a kappa value of 0.89. These results indicate a very strong level of agreement between the classification outputs and reference data (Kappa > 0.75), confirming that the land cover maps reliably represent actual field conditions.

Vegetation indices NDVI and NDLI

NDVI indices in 2016 and 2025

A comparison of the NDVI results between 2016 and 2025 revealed changes in the vegetation greenness structure in the study area. In 2016, high greenness classes (0.36–1.00) dominated, covering approximately 153,709.82 ha, particularly in forested and mountainous areas. By 2025, dominance shifted to the medium greenness class (0.26–0.35), with an area of approximately 68,750 ha, whereas high greenness declined to approximately 65,055 ha, indicating a reduction in vegetation greenness but not a loss of overall vegetation cover.

The areas of low to very low greenness and nonvegetated classes in 2025 remained relatively limited (approximately 10,020 ha and 4,767 ha, respectively), suggesting that these changes primarily reflect a decline in vegetation quality rather than large-scale conversion to nonvegetated land. Overall, the vegetation conditions in the study area generally remain good and relatively stable despite ongoing land use changes. The changes in the NDVI values in 2016 and 2025 are shown in Table 9.

NDLI index 2016 and 2025

A comparison of the NDLI results for 2016 and 2025 reveals changes in surface moisture and vegetation water conditions in the study area. In 2016, the moist NDLI class (0.2–0.4) dominated, covering approximately 108,561.64 ha, whereas very moist conditions (>0.4) were mainly limited to mangrove ecosystems and densely vegetated hilly areas, reflecting high moisture availability only in ecologically stable zones.

In 2025, dominance shifted toward high to very high NDLI values (≥0.5), indicating increased vegetation water content, evapotranspiration intensity, and latent heat exchange, with low NDLI values remaining concentrated in built-up and open areas. Overall, the NDLI dynamics from 2016 to 2025 suggest gradual and controlled land cover changes in North Gorontalo Regency, with no evidence of widespread vegetation moisture degradation. The changes in the NDLI values for 2016 and 2025 are shown in Table 10.

Accuracy test

Accuracy testing was performed to evaluate the suitability of the NDVI and NDLI classifications for representing land cover conditions in 2016 and 2025. The NDVI was used to distinguish vegetated and nonvegetated areas, whereas the NDLI represented land surface moisture conditions. Accuracy was assessed via validation sample points and confusion matrix analysis, with the NDVI accuracy results and corresponding OA and kappa values presented in Tables 11 and 12.

The NDVI accuracy results clearly improved from 2016-2025. In 2016, the NDVI achieved an overall accuracy of 92.64%, with a kappa coefficient of 0.85, indicating very strong agreement between the classification results and reference data (Rahmawati et al., 2025), although some nonvegetated areas were misclassified as vegetated. In 2025, the NDVI performance improved substantially, reaching an overall accuracy of 97.82% and a kappa value of 0.96, with more balanced producer and user accuracies across classes, indicating greater stability and accuracy in distinguishing vegetated and nonvegetated areas. The NDLI confusion matrices for 2016 and 2025

(a)

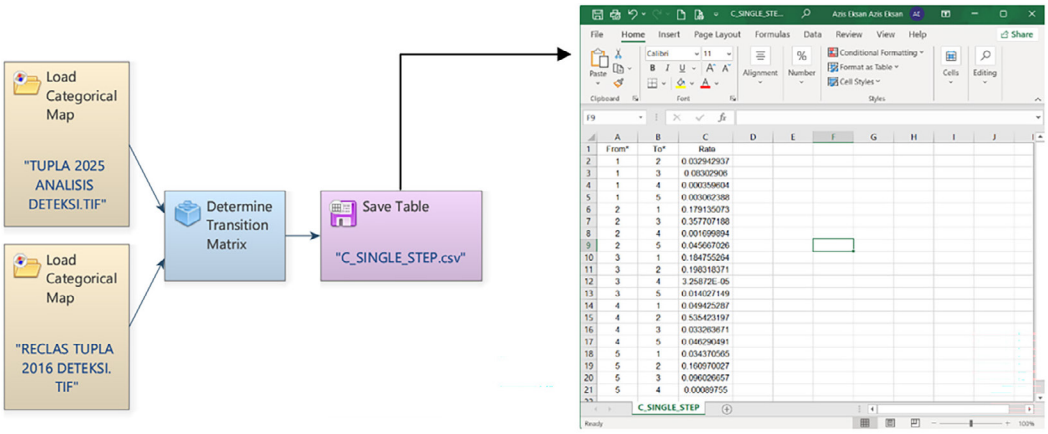
Load Categorical Map
"TUPLA 2025 ANALISIS DETEKSI.TIF"
Load Categorical Map
"RECLAS TUPLA 2016 DETEKSI. TIF"
Determine Transition Matrix
Save Table
"C_SINGLE_STEP.csv"
C_SINGLE_STEP

(b)

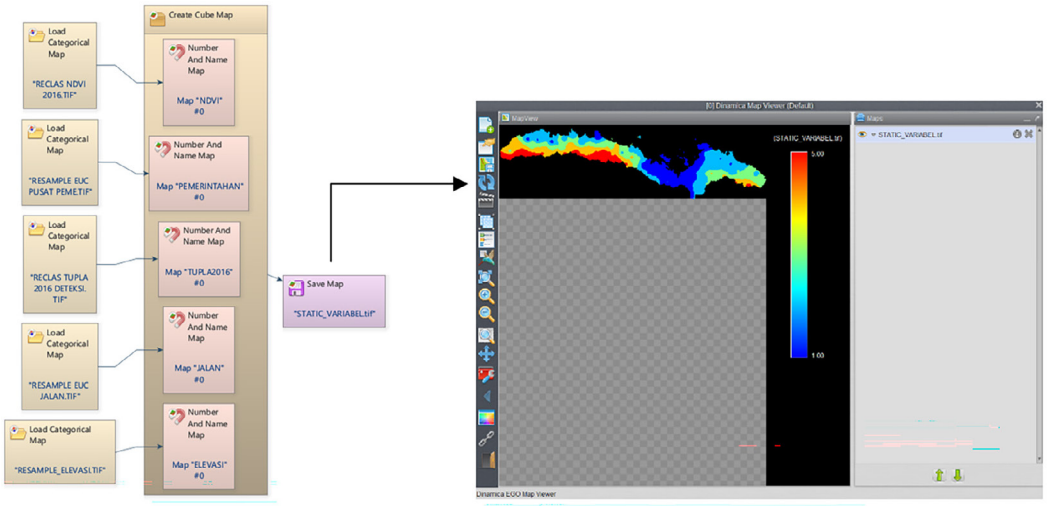
Create Cube Map
Load Categorical Map
"RECLAS NDVI 2016.TIF"
Load Categorical Map
"RESAMPLE EUC PUSAT PEMETIF"
Load Categorical Map
"RECLAS TUPLA 2016 DETEKSI. TIF"
Load Categorical Map
"RESAMPLE EUC JALAN.TIF"
Load Categorical Map
"RESAMPLE_ELEVASI.TIF"
Number And Name Map
Map "NDVI" #0
Number And Name Map
Map "PEMERINTAHAN" #0
Number And Name Map
Map "TUPLA2016" #0
Number And Name Map
Map "JALAN" #0
Number And Name Map
Map "ELEVASI" #0
Save Map
"STATIC_VARIABEL.tif"

(c)

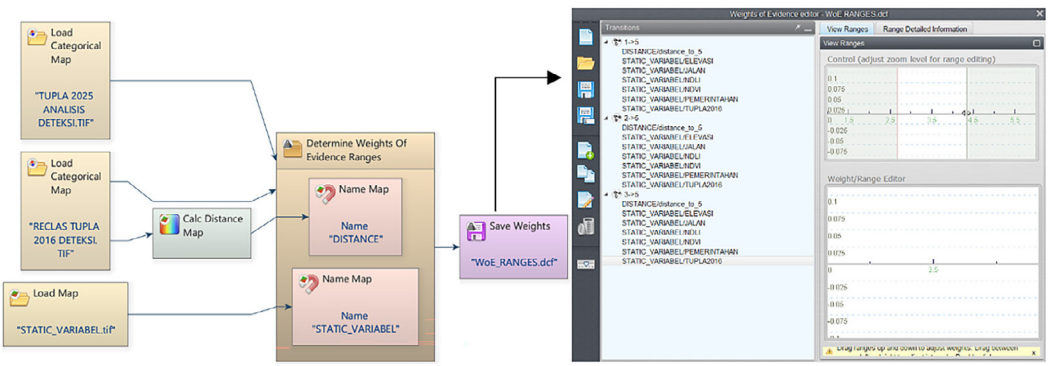
Load Categorical Map
"TUPLA 2025 ANALISIS DETEKSI.TIF"
Load Categorical Map
"RECLAS TUPLA 2016 DETEKSI. TIF"
Load Map
"STATIC_VARIABEL.tif"
Calc Distance Map
Determine Weights Of Evidence Ranges
Name Map
Name "DISTANCE"
Name Map
Name "STATIC_VARIABEL"
Save Weights
"WoE_RANGES.dcf"
Weights of Evidence editor - WoE RANGES.dcf
Transitions
View Ranges
Range Detailed Information

(d)

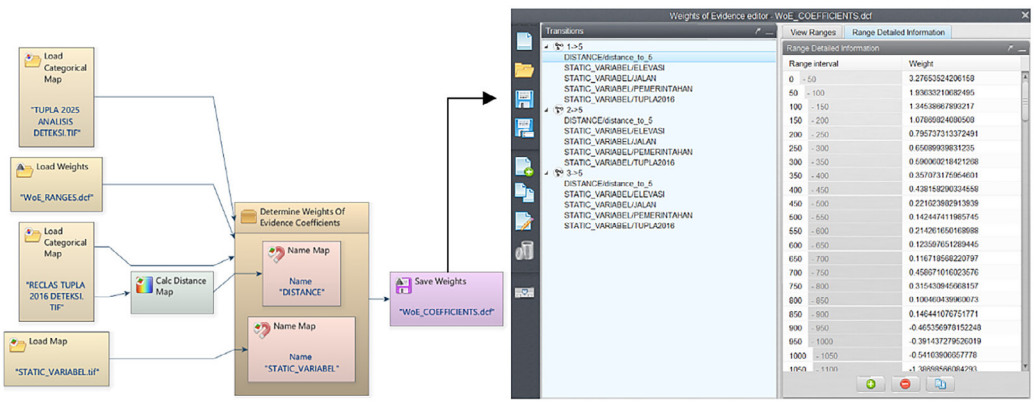
Load Categorical Map
"TUPLA 2025 ANALISIS DETEKSI.TIF"
Load Weights
"WoE_RANGES.dcf"
Load Categorical Map
"RECLAS TUPLA 2016 DETEKSI. TIF"
Load Map
"STATIC_VARIABEL.tif"
Calc Distance Map
Determine Weights Of Evidence Coefficients
Name Map
Name "DISTANCE"
Name Map
Name "STATIC_VARIABEL"
Save Weights
"WoE_COEFFICIENTS.dcf"
Weights of Evidence editor - WoE_COEFFICIENTS.dcf
Transitions
View Ranges
Range Detailed Information
Range interval
Weight

(e)

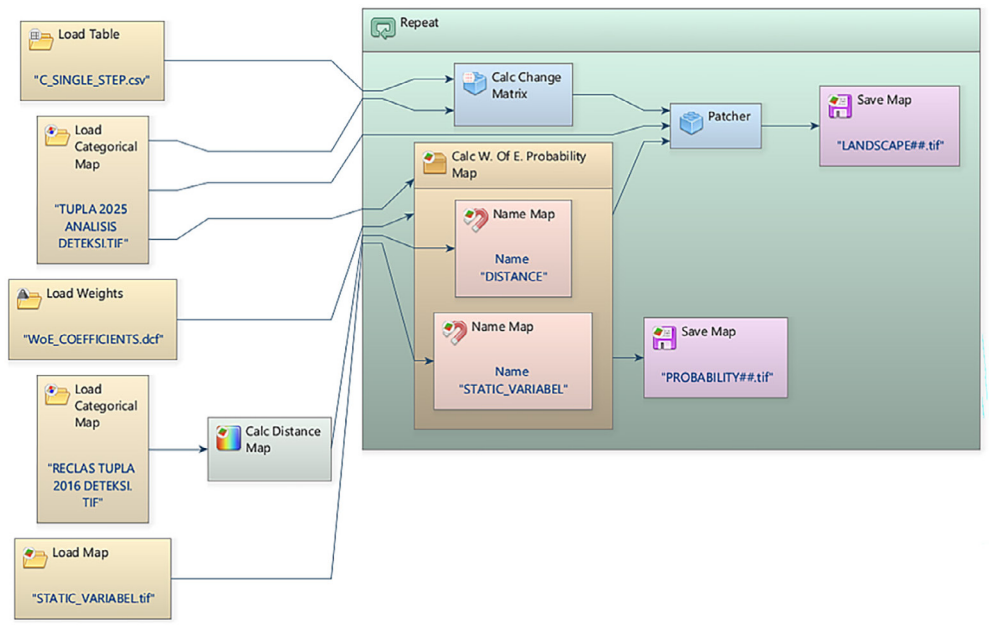

Figure 7. CLUE-S land use modeling with Dinamica EGO, (a) submodel transition matrix, (b) create cube map, (c) weights of evidence ranges, (d) weights of evidence coefficients, (e) simulation and scenario

Table 5. Land cover conditions in 2016 and 2025

Land cover classification	Area (Ha) 2016	Area (Ha) 2025	Area difference (Ha)	Land cover classification
Forest	100.006	102.171	+2.17	2.16
Agricultural area	35.081	26.364	-8.72	-24.85
Grassland/mixed vegetation	27.695	36.905	+9.21	33.26
Fishpond	287	156	-131	-45.64
Built-up land	1.790	3260	+1470	82.12
Grand total	171.852	171.852		

Note: Researcher analysis, 2025; value (+) → increase, value (-) → decrease.

Table 6. Land cover confusion matrix for 2016

Land cover classification	Land cover class	1	2	3	4	5	Total
Forest	1	791	4	0	0	6	801
Agricultural area	2	0	1125	23	18	0	1166
Built-up land	3	0	152	611	0	1	764
Fishpond	4	1	1	0	72	0	74
Grassland/mixed vegetation	5	35	28	0	0	1033	1096
Grand total		827	1310	634	90	1040	3901

are shown in Table 13. In addition, the OA values and kappa coefficients for the NDLI in 2016 and 2025 are shown in Table 14.

The NDLI accuracy results clearly improved from 2016 to 2025, with the overall accuracy increasing from 88.55% (Kappa = 0.77) to 95.73% (Kappa = 0.92), reflecting a more balanced classification of moist and dry areas and a more reliable representation of land surface moisture conditions. On the basis of its relatively high overall accuracy and kappa coefficient, the 2025 NDVI was selected

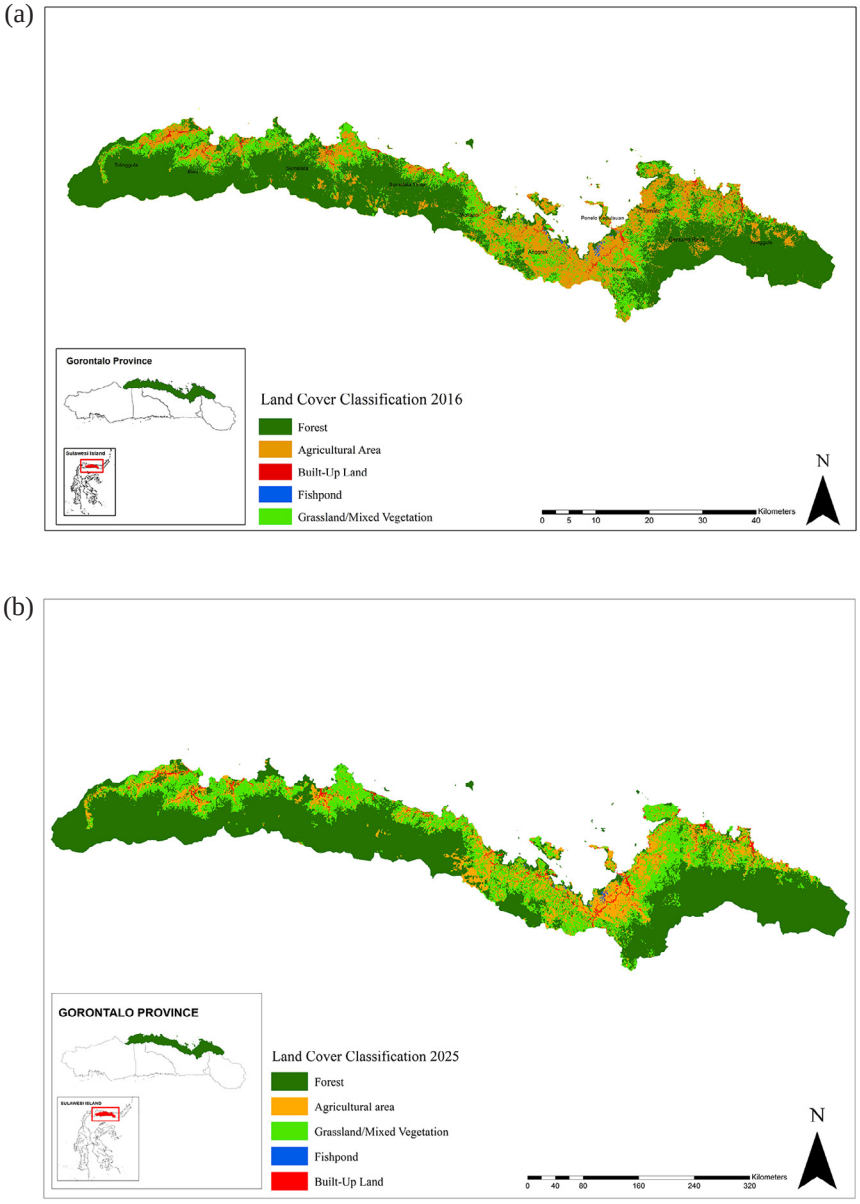

Figure 8. (a) Land cover conditions in 2016, (b) land cover conditions in 2025

Table 7. Confusion matrix for land cover in 2025

Land Cover Classification	Land Cover Class	1	2	3	4	5	Total
Forest	1	547	2	24	0	1	574
Agricultural Area	2	30	1397	21	0	65	1513
Built-Up Land	3	6	1	479	0	0	486
Fishpond	4	0	10	0	34	0	44
Grassland/Mixed Vegetation	5	1	106	3	0	708	818
Grand Total		584	1516	527	34	774	3435

Note: Researcher's analysis results, 2025.

as the primary input for land cover classification and CLUE-S-based modeling, whereas the NDLI was used as supporting information to strengthen environmental analysis and improve the reliability of spatial allocation and simulation results.

Table 8. Changes in the NDVI values in 2016 and 2025

NDVI Class	NDVI Value Range	Area in 2016 (Ha)	Area in 2025 (Ha)	Area Difference (Ha)	Change (%)	Overall Change
High Greenery	0.36 - 1.00	153,710	65,055	-88,655	-58	Significantly decreased
Moderate greenness	0.26 - 0.35	7,591	68,750	61,159	806	Increasing and becoming dominant
Low greenness	0.16 - 0.25	6,104	23,260	17,156	281	Increasing, second dominant
Very low greenness	-0.04 s/d 0.15	4,176	10,020	5,844	140	Limited increase
Nonvegetated land	-1 s/d -0.03	271	4,767	4,496	1,659	Remains small
Grand Total		171,85	171,852			

Note: Researcher analysis, 2025; value (+) → increase, value (-) → decrease.

Table 9. Changes in NDLI values for 2016 and 2025

NDLI Class	NDLI Value Range	Area in 2016 (Ha)	Area in 2025 (Ha)	Area Difference (Ha)	Percentage Change	Rate of Change
Very moist	> 0.4	74	61,953	61,879	84,178	Highly significant
Moist	0.2 - 0.4	108,562	61,175	-47,387	-44	Decreasing
Moderately Moist	0 - 0.2	51,290	27,333	-23,957	-47	Decreasing
Dry	-0.2 - 0	11,544	15,025	3,481	30	Limited increase
Very Dry	< -0.2	383	6,367	5,984	1,561	increased
Grand Total		171.852	171.852			

Note: Researcher analysis, 2025; value (+) → increase, value (-) → decrease.

Table 10. NDVI confusion matrix for 2016 and 2025

Year 2016	Prediction			Prediction	Prediction		
Reference	Vegetated	Nonvegetated	Total	Reference	Vegetated	Nonvegetated	Total
Vegetated	549	1	550	Vegetated	600	0	600
Nonvegetated	80	470	550	Nonvegetated	24	476	500
Total	628	471	1019		624	476	1076
N Value (Total Sample)			1100	N Value (Total Sample)			1100

Note: Researcher's analysis results, 2025.

Table 11. OA values and kappa coefficients for the NDVI in 2016 and 2025

Year	Class	Producer's Accuracy (PA)	User Accuracy (UA)	Overall Accuracy (OA)	Kappa
2016	Vegetated	99.82%	87.36%	92.64%	0.85
	Nonvegetated	85.45%	99.79%		
2025	Vegetated	100%	96.15%	97.82%	0.96
	Nonvegetated	95.20%	100%		

Note: Researcher's analysis results, 2025.

Direction and development of the city

Land cover conversion to built-up areas

The 2016–2025 raster transition map shows heterogeneous land cover changes across North Gorontalo Regency (Figure 6). Most areas, especially forests and hills in the south, remain unchanged (light pink), while new built-up areas (red) form linear corridors and small clusters along coastal lowlands and major roads. Built-up growth is concentrated around administrative centers–Kwandang, Anggrek, Gentuma Raya,

Table 12. NDLI confusion matrices for 2016 and 2025

Year 2016	Prediction			Year 2025	Prediction		
Reference	Moist	Dry	Total	Reference	Moist	Dry	Total
Moist	541	9	550	Moist	545	26	571
Dry	117	433	560	Dry	21	508	529
Total	658	442	974	Total	566	534	1053
N Value (Total Sample)			1100	N Value (Total Sample)			1100

Note: Researcher's analysis results, 2025

Table 13. OA values and kappa coefficients for the NDLI in 2016 and 2025

Year	Class	Producer's Accuracy (PA)	User's Accuracy (UA)	Overal Accuracy (OA)	Kappa
2016	Moist	98.36%	82.25%	88.55%	0.77
	Dry	78.73%	97.96%		
2025	Moist	95.45%	96.29%	95.73%	0.92
	Dry	96.03%	95.13%		

Note: Researcher's analysis results, 2025.

and Tomilito – indicating that agricultural land, mixed vegetation, and fishponds are mainly converted in highly accessible locations.

Directional distribution (standard deviational ellipse)

Urban growth direction was quantified using the directional distribution (standard deviational ellipse – SDE) method with one standard deviation, representing approximately 68% of the spatial distribution of growth points. The resulting ellipse exhibits a rotation angle of 99.11°, indicating a dominant east–southeast to west–northwest orientation. The major axis (55,822 m) is substantially larger than the minor axis (7,606 m), yielding an anisotropy ratio of approximately 7.34:1, which confirms a strongly elongated and directional expansion pattern. The spatial extent of the dominant growth corridor covers approximately 1332.45 km², highlighting the broad geographic influence of urban expansion. The mean center of growth is located near the administrative core, suggesting that development is spatially anchored to institutional and service centers.

Driving factors

Euclidean distance analysis shows that proximity to main roads and government centers strongly shapes spatial development patterns. Areas near these features exhibit higher land conversion, forming continuous development corridors, while remote areas show limited change, highlighting accessibility as a key driver of urban expansion. Elevation reclassification indicates that development is mainly concentrated in low to moderate zones (55–603 m), with medium elevations (603–901 m) serving as transitional areas and high elevations (901–2052 m) constraining growth and retaining forest cover. This north–south topographic gradient directs urban expansion toward coastal lowlands. NDVI analysis between 2016 and 2025 reveals declining vegetation in western and central areas, coinciding with built-up expansion, whereas eastern regions maintain moderate to high vegetation, indicating progressive conversion of vegetated land along primary development axes.

Direction and pattern of urban development

The map of growth potential and development direction of north Gorontalo Regency in 2025 is the result of the integration of land use changes, NDVI, distance to main roads, and distance to government centers, which were subsequently classified into low, medium, and high potential categories. High-potential zones are concentrated around government centers and along the main road network, while medium-potential zones follow transportation corridors, and low-potential zones are located in peripheral areas, slopes, and regions distant from service centers.

Standard deviational ellipse analysis indicates that built-up area development exhibits a dominant east–southeast orientation with a linear pattern following transportation corridors and coastal areas, reflecting a ribbon development

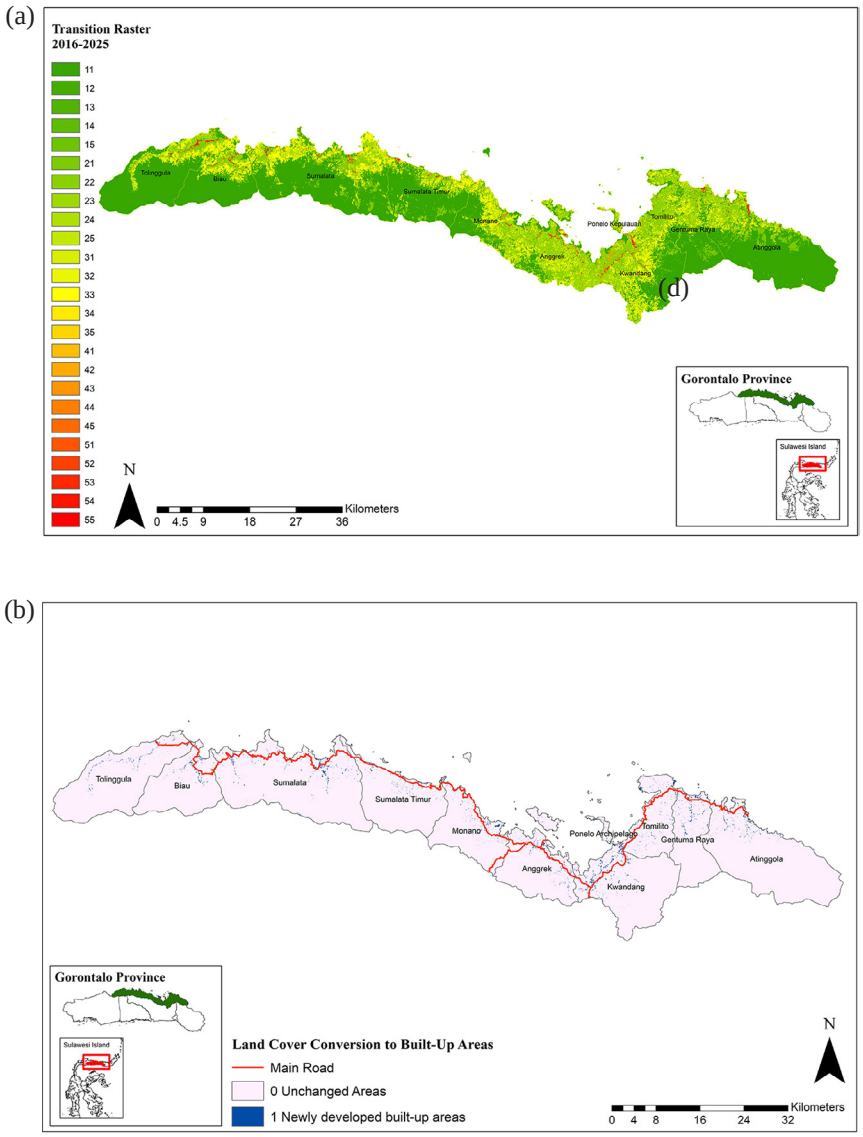

Figure 9. (a) Raster transition map of land cover for 2016–2025, (b) built-up areas 2016-2025

Table 14. Standard deviational ellipse parameters of urban growth (2016–2025)

Parameter	Value	Unit	Interpretation
CenterX	461,793.38	m	X-coordinate of growth centroid
CenterY	98,391.52	m	Y-coordinate of growth centroid
XStdDist	55,822.18	m	Major axis (maximum spatial variance)
YStdDist	7,605.81	m	Minor axis (minimum spatial variance)
Rotation	99.11	Degrees	Dominant orientation of urban growth
Axis Ratio	7.34	–	Degree of anisotropy (elongation)
Ellipse Area	1332.45	km²	Spatial extent of dominant growth

Note: Researcher's analysis results, 2025

pattern. This pattern aligns with Hoyt's sector theory (1939) and is reinforced by NDVI and NDLI results, which show the gradual conversion of vegetated land into built-up areas along the main development axis.

Overall, the analysis demonstrates a tendency for urban development to be concentrated in areas with high accessibility and proximity to public service centers. This development pattern suggests that the presence of main road networks serves as the primary controlling factor for land transformation, whereas elevation, vegetation, and ecological conditions act as natural limiting factors.

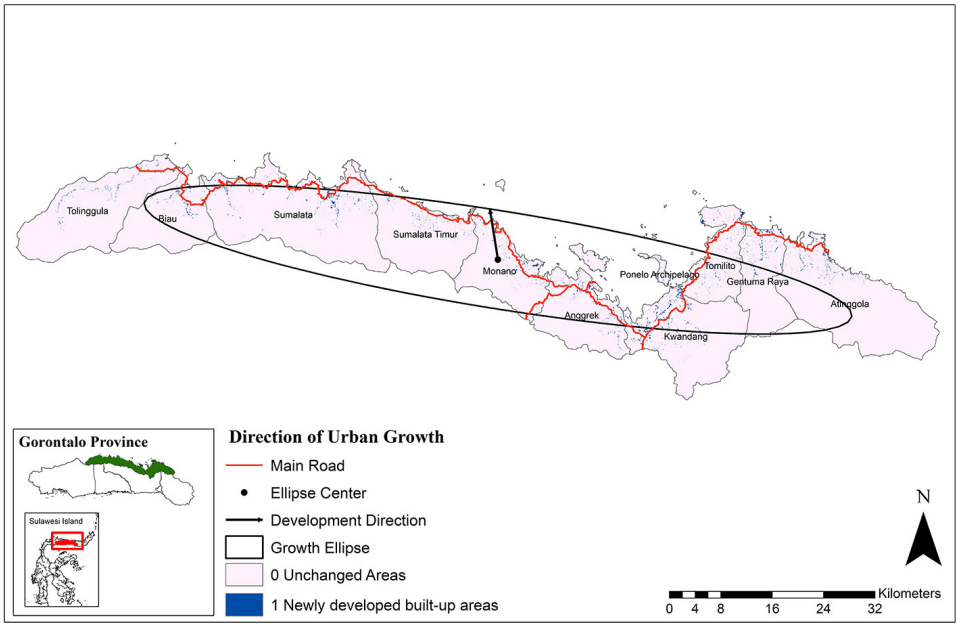

Figure 10. Direction of urban growth map

Dominant factors of land cover change and urban development

Binary logistic regression

Binary logistic regression was conducted in SPSS to assess the influence of driving factors on land cover change, with land cover change coded as a binary dependent variable (1 = change, 0 = no change) and biophysical and accessibility variables as predictors. The results indicate that the NDVI and distance to roads significantly influenced land cover change ($p < 0.001$), with the NDVI showing a negative coefficient (–2.477) that reflects a decreasing likelihood of change with increasing vegetation density. In contrast, distance to government centers and elevation were not significant. Accordingly, the NDVI and distance to roads were identified as the primary driving factors and were used in the CLUE-S modeling, as presented in Table 16.

The feasibility of the binary logistic regression model in this study was evaluated via several statistical indicators, namely, the Hosmer–Lemeshow test, the pseudodetermination coefficient (Nagelkerke R square), and the receiver operating characteristic (ROC) curve. The Hosmer-Lemeshow test showed a significance value greater than 0.05, indicating that the model has a good fit between the observed and predicted values. The Nagelkerke R square value indicates that the independent variables used are able to explain variations in land cover change at an adequate level (C.A. Jiang et al., 2015). The Hosmer-Lemeshow test results (Sig) anda Nagelkerke R square values are shown in Table 17. In addition, the ROC curve is shown in Figure 12.

The Hosmer-Lemeshow test produced a significance value of 0.087 (>0.05), indicating a good model fit with no significant difference between the observed and predicted values. The Nagelkerke R square value of 0.155 suggests that approximately 15.5% of land cover change variation is explained by the independent variables, implying that additional factors outside the model also influence land cover dynamics. Model evaluation via the ROC curve yielded an AUC value of 0.707, indicating a fairly good and reliable ability of the binary logistic regression model to distinguish between areas that experienced land cover change and those that did not.

The logistic regression results revealed that among the four tested driving factors NDVI, distance to roads, distance to government centers, and elevation NDVI and distance to roads had the most significant influences on land cover change. Nevertheless, all four variables were incorporated into the CLUE-S model in Dinamica EGO to ensure that both dominant and supporting factors were considered in the spatial allocation of land cover change.

(a)

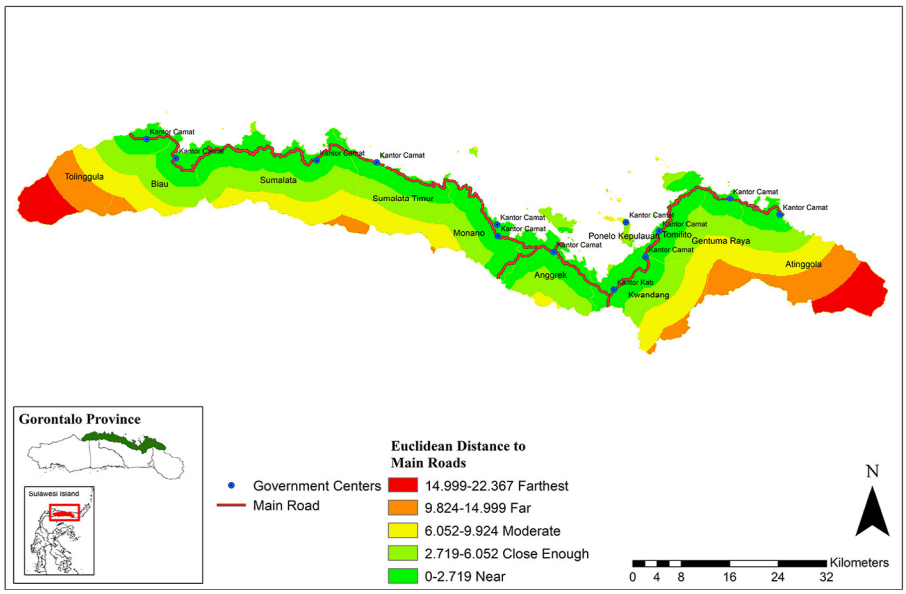
Tolinggula
Biau
Sumalata
Sumalata Timur
Monano
Anggrek
Ponelo Kepulauan
Tomilito
Gentuma Raya
Atinggola
Kwandang
Kantor Camat
Kantor Kab
Gorontalo Province
Sulawesi Island
Government Centers
Main Road
Euclidean Distance to Main Roads
14.999-22.367 Farthest
9.824-14.999 Far
6.052-9.924 Moderate
2.719-6.052 Close Enough
0-2.719 Near
N
Kilometers
0 4 8 16 24 32

(b)

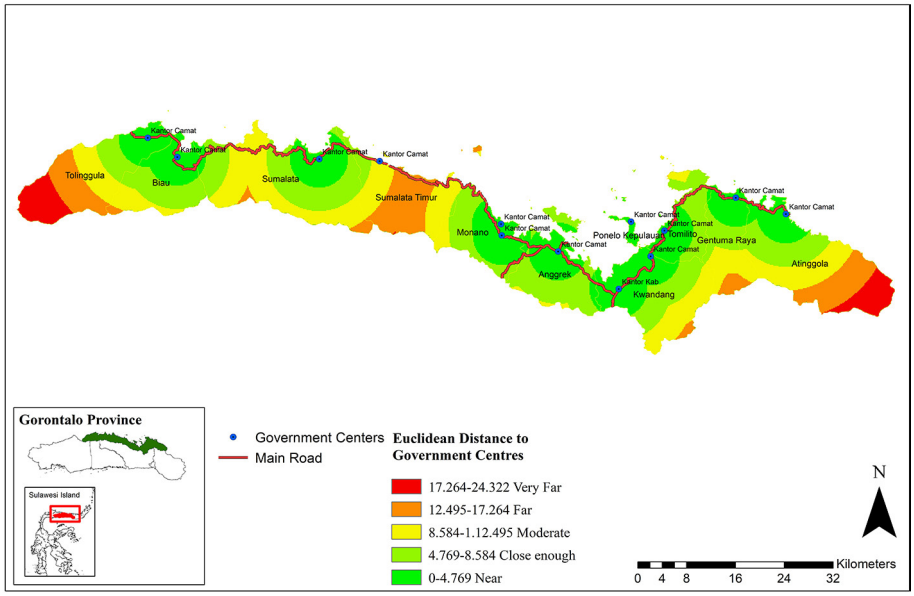
Tolinggula
Biau
Sumalata
Sumalata Timur
Monano
Anggrek
Ponelo Kepulauan
Tomilito
Gentuma Raya
Atinggola
Kwandang
Kantor Camat
Kantor Kab
Gorontalo Province
Sulawesi Island
Government Centers
Main Road
Euclidean Distance to Government Centres
17.264-24.322 Very Far
12.495-17.264 Far
8.584-1.12.495 Moderate
4.769-8.584 Close enough
0-4.769 Near
N
Kilometers
0 4 8 16 24 32

(c)

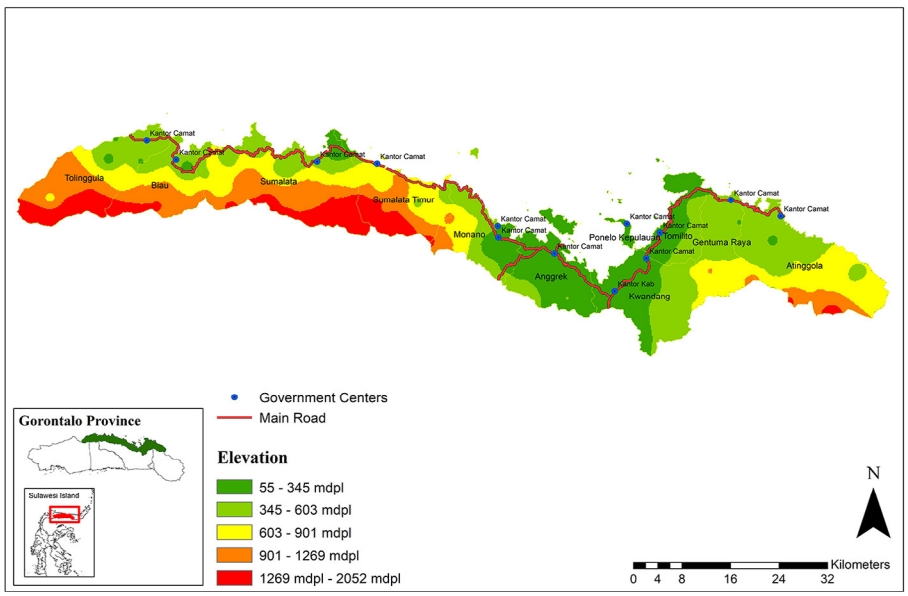
Tolinggula
Biau
Sumalata
Sumalata Timur
Monano
Anggrek
Ponelo Kepulauan
Tomilito
Gentuma Raya
Atinggola
Kwandang
Kantor Camat
Kantor Kab
Gorontalo Province
Sulawesi Island
Government Centers
Main Road
Elevation
55 - 345 mdpl
345 - 603 mdpl
603 - 901 mdpl
901 - 1269 mdpl
1269 mdpl - 2052 mdpl
N
Kilometers
0 4 8 16 24 32

(d)

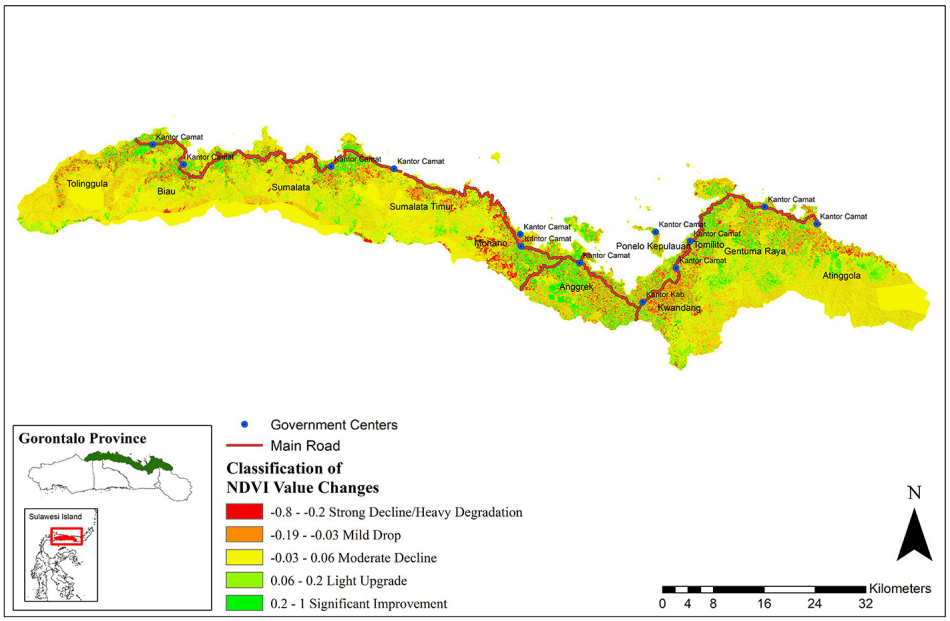

Figure 11. (a) Euclidean distance to main roads, (b) Euclidean distance to government centers, (c) elevation map, and (d) map of the NDVI value classification for 2016-2025

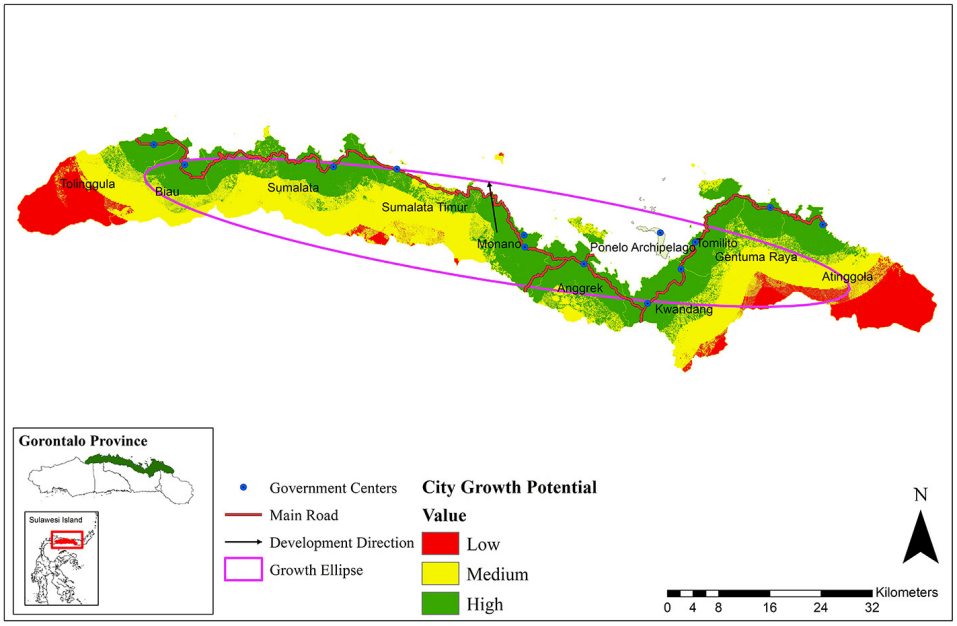

Figure 12. Development direction of North Gorontalo

Table 15. Logistic regression results of factors driving land cover change

Variables in the Equation							
		B	S.E.	Wald	df	Sig.	Exp(B)
Step 1[a]	NDVI	-2.477	.455	29.686	1	<.001	.084
	Road	.000	.000	50.698	1	<.001	1.000
	Government Centre	.000	.000	.039	1	.844	1.000
	Elevation	.000	.000	.313	1	.576	1.000
	Road	1.541	.224	47.257	1	<.001	4.667
a. Variable(s) entered on step 1: NDVI, Road, Government Centre, Elevation.							

Table 16. Hosmer-Lemeshow test results (Sig)

Hosmer and Lemeshow test				Model summary Nagelkerke R square values		
Step1	Chi-square	df	Sig.	-2 Log likelihood	Cox & Snell R square	Nagelkerke R square
	13.814	8	.087	1385.028[a]	.116	.155
				Estimation terminated at iteration number 4 because parameter estimates changed by less than .001.		

Note: sResearcher's analysis results, 2025

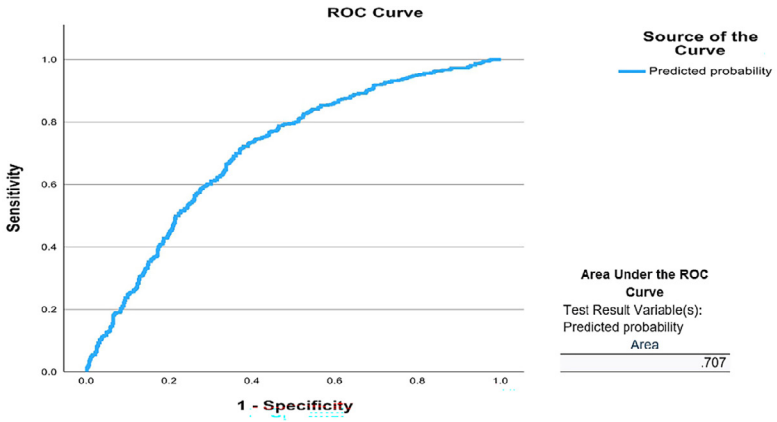

Figure 13. ROC curve

CLUE-S modeling

Business-as-usual (BAU) scenario

On the basis of Figure 9, model validation was performed by comparing the simulated map and the actual 2025 land cover map, which was simplified into urban and nonurban classes. The results revealed excellent model performance, with an overall accuracy of 98.79% and a kappa coefficient of 0.78. Although all the urban areas were identified (producer accuracy 100%), there was a tendency for urban overprediction (user accuracy 64.78%), whereas the nonurban class had very high and consistent accuracy. The CLUE-S modeling accuracies are shown in Table 18.

The simulation results indicate that built-up areas still exist within protected areas in 2025, likely reflecting the existing conditions before the RTRW was enacted. This finding reflects the limitations of spatial planning policies in correcting existing conditions, necessitating further temporal analysis to assess the effectiveness of the RTRW more comprehensively.

Protected areas ecological function scenario based on regency spatial plan

Scenario 2 was developed using a policy-based spatial constraint approach to assess how protected area regulations influence the direction and pattern of built-up area development in north Gorontalo Regency.

The analysis shows that portions of built-up areas have developed within protected zones, particularly along coastal areas and river corridors, with Windu Village in Biau Subdistrict serving as a representative example. This indicates that pressure on protected areas existed prior to the simulation period. Visual interpretation of Google Earth imagery from 2004 reveals that built-up land was already present and continued to expand until 2023, suggesting that settlement development occurred before the implementation of the Regional Spatial Plan (RTRW). Even after the RTRW was formally enacted in 2013, built-up expansion persisted, reflecting the limited effectiveness of spatial planning implementation.

These conditions highlight challenges in urban governance related to spatial planning compliance in ecologically sensitive areas. Weak policy enforcement, limited institutional capacity, and increasing residential and economic pressures have resulted in the RTRW functioning largely as a normative framework without effective local implementation. Therefore, strengthened policy enforcement, improved institutional coordination, and more integrated spatial management are essential to balance urban growth with environmental protection.

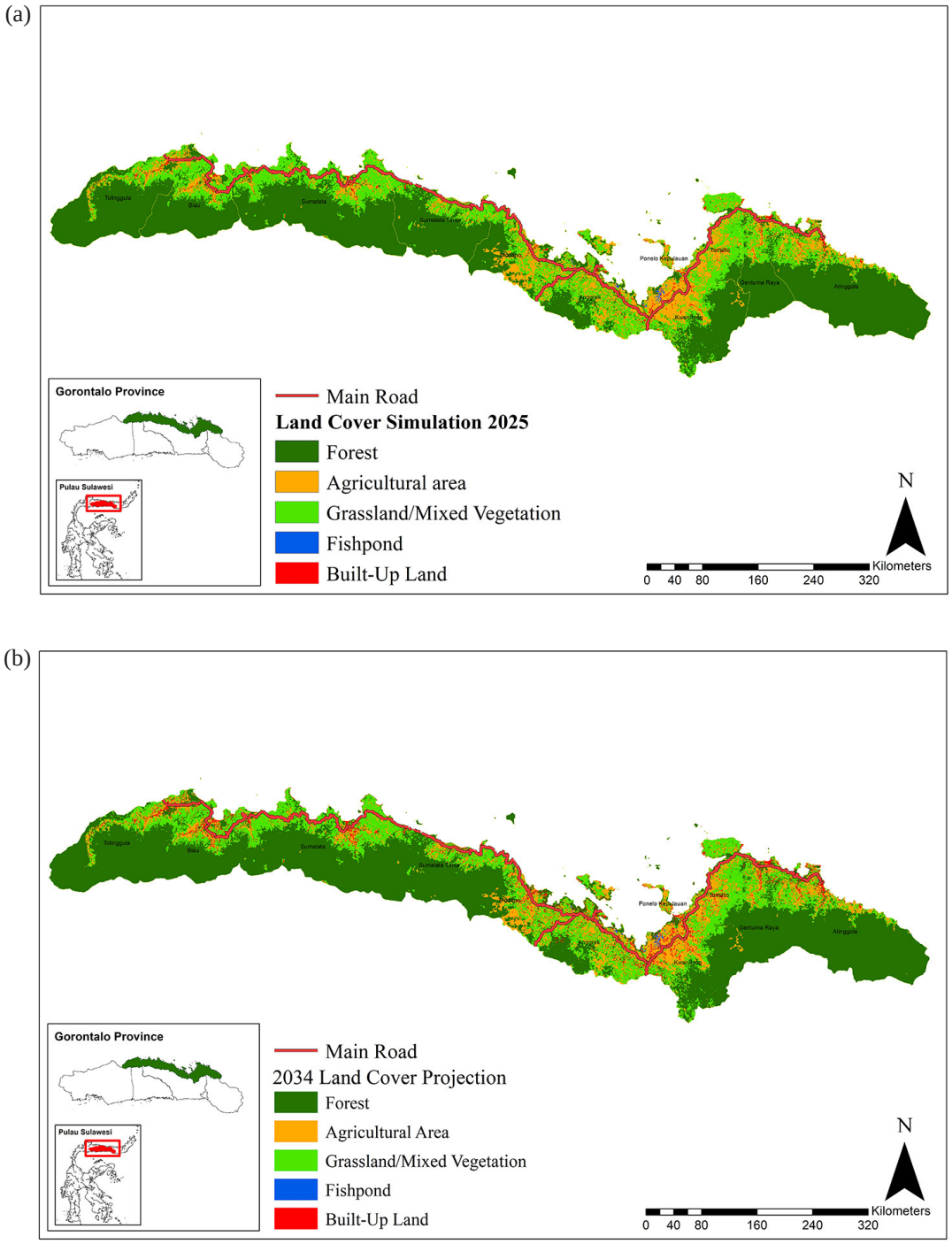

Figure 14. (a) 2025 land cover simulation map and (b) 2034 land cover projection map

Table 17. CLUE-S modeling accuracy

Indicator	Value
Overal accuracy	98.79%
Kappa coefficient	0.78 (very good))
Producer's accuracy urban	100%
Ucer's accuracy urban	64.78%
Producer's accuracy non-urban	98.77%
User's accuracy non-urban	100%

Note: Researcher's analysis results, 2025.

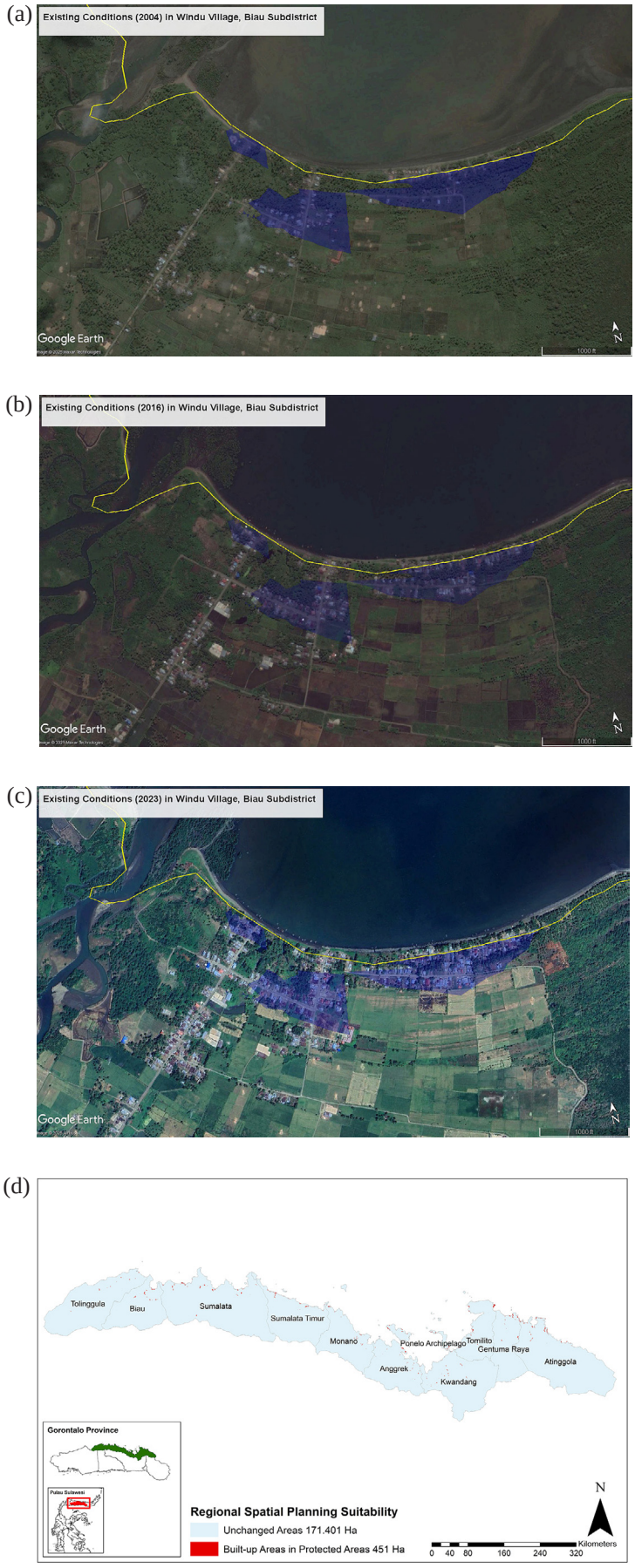

Figure 15. (a) Existing condition 2004, (b) existing condition 20016, (c) existing condition 2023, (d) regional spatial planning suitability map

CONCLUSIONS

Between 2016 and 2025, North Gorontalo Regency experienced significant built-up expansion, primarily converting agricultural land and fishponds along transportation corridors and coastal zones, driven by accessibility and biophysical suitability rather than administrative planning. Logistic regression identifies vegetation (NDVI) and proximity to roads as primary drivers, with elevation and distance to government centers as secondary constraints, while CLUE-S simulations confirm a spatially directed East–Southeast growth pattern. Overlay with the Regional Spatial Plan (RTRW) reveals that some urban expansion exceeds designated zones, including protected areas, highlighting the limits of static planning tools. Despite model uncertainties and the exclusion of dynamic socio-economic variables, CLUE-S captures general spatial trends, suggesting that integrating remote sensing indicators (NDVI–NDLI) and simulation outputs into RTRW evaluation can improve early detection of development pressure, zoning control, and adaptive, evidence-based spatial planning.

REFERENCES

1. Akın, A., Erdoğan, N., Berberoğlu, S., Çilek, A., Erdoğan, A., Donmez, C., & Şatir, O. (2022). Evaluating the efficiency of future crop pattern modelling using the CLUE-S approach in an agricultural plain. *Ecological Informatics*, *71*. https://doi.org/10.1016/j.ecoinf.2022.101806
2. Ardianto, G., Segah, H., Aguswan, Y., Triyadi, A., & Siska, G. (2022). Analisis Perubahan Tutupan Lahan Menggunakan Citra Sentinel 2 Areal Laboratorium Alam Hutan Gambut CIMTROP Universitas Palangka Raya. In *Journal of Peat Science and Innovation* (Vol. 1). http://earthexplorer.usgs.gov
3. Arisondang, V., Sudarsono, B., & Prasetyo, Y. (2015). Klasifikasi Tutupan Lahan Menggunakan Metode Segmentasi Berbasis Algoritma Multiresolusi (Studi Kasus Kabupaten Purwakarta, Jawa Barat). *Jurnal Geodesi Undip*, *4*(1).
4. Azizah Nazhifah, S., Putri, A., & Kiftiyani, U. (2025). Comparative evaluation of NDVI-based vegetation classification using rule-based approach and random forest models. *Jurnal Pendidikan Teknologi Informasi*, *9*(2), 22–32.
5. Badan Standardisasi Nasional. (2010). *Standar Nasional Indonesia Klasifikasi penutup lahan SNI 7645:2010*. www.bsn.go.id
6. Baderan, D. W. K. (2017). Distribusi Spasial dan Luas Kerusakan Hutan Mangrove di Wilayah Pesisir Kwandang Kabupaten Gorontalo Utara Provinsi Gorontalo. *Jurnal GeoEco*, *3*(1), 1–8.
7. BPS. (2025). Provinsi Gorontalo Dalam Angka 2025. In *2025*.
8. Burgess, E. W. (1925). The growth of the city: an introduction to a research project. *American Sociological Society*.
9. Cao, H., & Kim, E. (2025). Analysis of influencing factors on spatial distribution characteristics of traditional villages in the Liaoxi corridor. *Land*, *14*(8). https://doi.org/10.3390/land14081572
10. da Rocha de Souza, E. M. F., Gomes, A. A. T., & Viegas, V. S. (2025). Urban growth in metropolitan regions using dynamic modeling by cellular automata: a comparative analysis between Brazil and Portugal. *International Conference on Geographical Information Systems Theory, Applications and Management, GISTAM - Proceedings*, (Gistam), 142–149. https://doi.org/10.5220/0013205000003935
11. Dharma, F., Aulia, A., Shubhan, F., & Ridwana, R. (2022). Pemanfaatan Citra Sentinel - 2 Dengan Metode NDVI Untuk Perubahan Kerapatan Vegetasi Mangrove Di Kabupaten Indramayu. *J Pendidikan Geografi Undiksha*, *10*(2), 155–165.
12. Eastman, C.I., Gazda, C.J., Burgess, H.J., Crowley, S.J., & Fogg, L.F. (2005). *Advancing circadian rhythms before eastward flight: a strategy to prevent or reduce jet lag* (Vol. 28, Number 1).
13. Ewing, R. (1997). Is Los Angeles-style sprawl desirable? *Journal of the American Planning Association*, *63*(1), 107–126. https://doi.org/10.1080/01944369708975728
14. Gil Pontius Jr, R., & Schneider, L.C. (2001). Land-cover change model validation by an ROC method for the Ipswich watershed, Massachusetts, USA. *Ecosystems and Environment*, 85.
15. Giofandi, E.A., Sekarjati, D., Tjahjono, B., Hidiya, M., & Mulyono, M.R. (2025). Long-term land use dynamics and scenario-based planning for sustainable development in the dumai river basin, Western Indonesia. *Journal of Umm Al-Qura University for Applied Sciences*. https://doi.org/10.1007/s43994-025-00296-5
16. Gonzales, J.E.V., & Hopfgartner, K. (2024). Modeling future projections of land use and land cover in the Kakataibo territory. *International archives of the photogrammetry, remote sensing and spatial information sciences - ISPRS archives*, *48*(3), 571–576. https://doi.org/10.5194/isprs-archives-XLVIII-3-2024-571-2024
17. Harris, C.D., & Ullman, E.L. (1945). The nature of cities. *The Annals of the American Academy of Political and Social Science*, *242*(1), 7–17. https://doi.org/10.1177/000271624524200103

18. Hoyt, H. (1939). *The structure and growth of residential neighborhoods in American Cities*. Federal Housing Administrator.
19. Jiang, C.A., Wu, Q.T., Goudon, R., Echevarria, G., & Morel, J.L. (2015). Biomass and metal yield of co-cropped Alyssum murale and Lupinus albus. *Australian Journal of Botany*, *63*(2), 159–166. https://doi.org/10.1071/BT14261
20. Jiang, W., Chen, Z., Lei, X., Jia, K., & Wu, Y. (2015). Simulating urban land use change by incorporating an autologistic regression model into a CLUE-S model. *Journal of Geographical Sciences*, *25*(7), 836–850. https://doi.org/10.1007/s11442-015-1205-8
21. Juniyanti, L., Prasetyo, L. B., Aprianto, D. P., Purnomo, H., & Kartodihardjo, H. (2020). Land-use/land cover change and its causes in Bengkalis Island, Riau Province (from 1990-2019). *Jurnal Pengelolaan Sumberdaya Alam Dan Lingkungan*, *10*(3), 419–435. https://doi.org/10.29244/jpsl.10.3.419-435
22. Kawamuna, A., Suprayogi, A., & Putra Wijaya, A. (2017). Analisis Kesehatan Hutan Mangrove Berdasarkan Metode Klasifikasi NDVI Pada Citra Sentinel-2 (Studi Kasus: Teluk Pangpang Kabupaten Banyuwangi). *Jurnal Geodesi Undip Januari*, 6(1). https://scihub.copernicus.eu/
23. Latue, P.C., Septory, J.S.I., & Rakuasa, H. (2023). Perubahan Tutupan Lahan Kota Ambon Tahun 2015, 2019 dan 2023. *JPG (Jurnal Pendidikan Geografi)*, *10*(1), 177–186. https://doi.org/10.20527/jpg.v10i1.15472
24. Manel, S., Ceri Williams, H., & Ormerod, S.J. (2001). Evaluating presence-absence models in ecology: The need to account for prevalence. *Journal of Applied Ecology*, *38*(5), 921–931. https://doi.org/10.1046/j.1365-2664.2001.00647.x
25. Marlina, D. (2022). Klasifikasi Tutupan Lahan pada Citra Sentinel-2 Kabupaten Kuningan dengan NDVI dan Algoritme Random Forest. *STRING (Satuan Tulisan Riset Dan Inovasi Teknologi)*, *7*(1), 41. https://doi.org/10.30998/string.v7i1.12948
26. Meena, S.R., Mishra, B.K., & Piralilou, S.T. (2019). A hybrid spatial multi-criteria evaluation method for mapping landslide susceptible areas in Kullu valley, Himalayas. *Geosciences (Switzerland)*, *9*(4). https://doi.org/10.3390/geosciences9040156
27. Nagendra, H., Tucker, C., Carlson, L., Southworth, J., Karmacharya, M., & Karna, B. (2004). Monitoring parks through remote sensing: Studies in Nepal and Honduras. *Environmental Management*, *34*(5), 748–760. https://doi.org/10.1007/s00267-004-0028-7
28. Novianti, T.C. (2021). Klasifikasi Landsat 8 Oli Untuk Tutupan Lahan Di Kota Palembang Menggunakan Google Earth Engine. *Jurnal Swarnabhumi*, *6*(1). http://code.earthengine.google.com/
29. Nursaputra, M., Putra Pahar, S.P., & Chairil, A. (2021). Identification of drought level using Normalized Difference Latent Heat Index in the South Coast of South Sulawesi Province. *IOP Conference Series: Earth and Environmental Science*, *807*(2). https://doi.org/10.1088/1755-1315/807/2/022032
30. P.12/Menhut-II. (2012). *Peraturan Menteri Kehutanan Republik Indonesia Nomor P.12/Menhut-II/2012*. www.djpp.depkumham.go.id
31. Pandapotan Sinurat, T., Munibah, K., Dwi Putro Tejo Baskoro, dan, Kehutanan dan Lingkungan Hidup, D., Raya Bonandolok, J.K., & Perkantoran Purba Dolok-Doloksanggul Kab Humbang Hasundutan Prov Sumatera Utara, K. (2015). *Modeling Land-Use Change in Humbang Hasundutan District Using Clue-S*. *17*(2), 75–82.
32. Pinto, L.V., Inácio, M., & Pereira, P. (2025). *MetodeX Protokol untuk memodelkan skenario penggunaan lahan di masa depan dengan menggunakan Dinamica-EGO "*, *14*.
33. Purboyo, A.A., Ramadhan, A.H., Safitri, E., Ridwana, R., & Himayah, S. (2021). Identifikasi Ruang Terbuka Hijau Menggunakan Metode Normalized Difference Vegetation Index Di Kota Depok. *Jurnal Sains Informasi Geografi*, *4*(1). https://doi.org/10.31314/j
34. Putri, E.S., Widiasari, A., Karim, R.A., Somantri, L., & Ridwana, R. (2021). Pemanfaatan Citra Sentinel-2 Untuk Analisis Gunung Manglayang. *Jurnal Jurusan Pendidikan Geografi*, *9*(2), 133–143.
35. Rahmawati, S.S., Setyowati, R., Ramlah, Azizah, S.N., Ardiansyah, R.M.Y., & Saikhu, A. (2025). Pemodelan Perubahan Lahan Dan Tutupan Lahan Berbasis Markov-Chain Di Kabupaten Gunung Kidul. *Jurnal Tanah Dan Sumberdaya Lahan*, *12*(2), 417–424. https://doi.org/10.21776/ub.jtsl.2025.012.2.19
36. Rakhmat Awaliyan, M., Yohanes Budi Sulistioadi, dan, Pemantapan Kawasan Hutan Wialayh Samarinda, B.I., Kehutanan, F., & Mulawarman, U. (2018). *Klasifikasi Penutupan Lahan Pada Citra Satelit Sentinel-2A Dengan Metode Tree Algorithm* (Vol. 2, Number 2).
37. Rakuasa, H., & Pakniany, Y. (2022). Spatial Dynamics of Land Cover Change in Ternate Tengah District, Ternate City, Indonesia. *Forum Geografi*, *36*(2). https://doi.org/10.23917/forgeo.v36i2.19978
38. Riaz, M.T., Riaz, M.T., Rehman, A., Bindajam, A.A., Mallick, J., & Abdo, H.G. (2024). An integrated approach of support vector machine (SVM)

and weight of evidence (WOE) techniques to map groundwater potential and assess water quality. *Scientific Reports*, *14*(1). https://doi.org/10.1038/s41598-024-76607-3

39. Setiawan, M.S., & Rijal, S. (2024). *Penyusunan Model Volume Hutan Alam dengan menggunakan Sentinel 2A di Hutan Pendidikan Universitas Hasanuddin*. *1*(1), 1–13.
40. Syifa Putri, E., Widiasari, A., Karim, R. A., Somantri, L., & Ridwana, R. (2021). Pemanfaatan Citra Sentinel-2 Untuk Analisis Kerapatan Vegetasi Di Wilayah Gunung Manglayang. *Jurnal Pendidikan Geografi Undiksha*, *9*(2), 133–143. https://doi.org/10.23887/jjpg.v9i2.35357
41. Varnier, M., & Weber, E. J. (2025). Evaluating the accuracy of land-use change models for predicting vegetation loss across Brazilian biomes. *Land*, *14*(3), 1–25. https://doi.org/10.3390/land14030560
42. Wahdaniah, Sukirman Rahim, I. B. (2022). Dampak Hutan Tanaman Industri Terhadap Perubahan Tutupan Lahan Hutan Dan Kondisi Sosial Ekonomi Masyarakat. *Journal of Forestry Research*, *5*(1).
43. Wahrudin, U., Atikah, S., Habibah, A. Al, Paramita, Q. P., Tampubolon, H., Sugandi, D., & Ridwana, R. (2019). Pemanfaatan Citra Landsat 8 Untuk Identifikasi Sebaran Kerapatan Vegetasi Di Pangandaran. *Jurnal Kajia Ilmu Dan Pendidikan Geografi*, 90–101.
44. Warlina, L. (2011). Pemodelan Perubahan Guna Lahan (Kasus Kabupaten Majalengka). *Jurnal Tata Loka*, *13*(4).